UNIVERSITY OF PADOVA

Department of Physics and Astronomy 'Galileo Galilei'
Master's Degree in Physics

Master's Thesis

ASYMPTOTIC BEHAVIOR OF LINKED LOOPS

Supervisor:
Prof. Enzo Orlandini

Thesis by: Andrea Bonato

Academic Year: 2017/2018

Contents

List of Figures

Chapter 1

Introduction

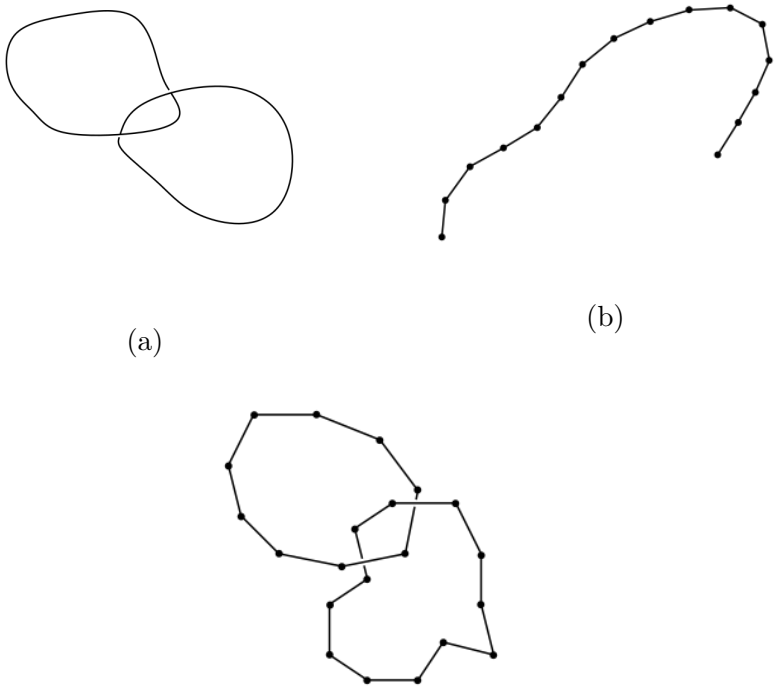

(a) (b) (c)

Figure 1.1: **(a)** Two unknotted loops linked with the topology of an Hopf link (in $\mathbb{R}^3$); it is the simplest nontrivial example of link. **(b)** A polymer chain is a sequence of connected units called monomers. **(c)** The object of interest: a link with the Hopf topology made by two polymer loops.

The purpose of this work is to investigate the asymptotic behavior of two unknotted linked polymer loops, closed chains composed of repeated and connected units called monomers, having the topology of the Hopf link, in 3 dimensions (figure 1.1).
A link is a collection of two or more loops linked to each other and, as such, it can be seen as the natural generalization of the concept of knot. Hence, to approach our problem, the starting point is what is known about the asymptotic behavior of polymer loops and walks.

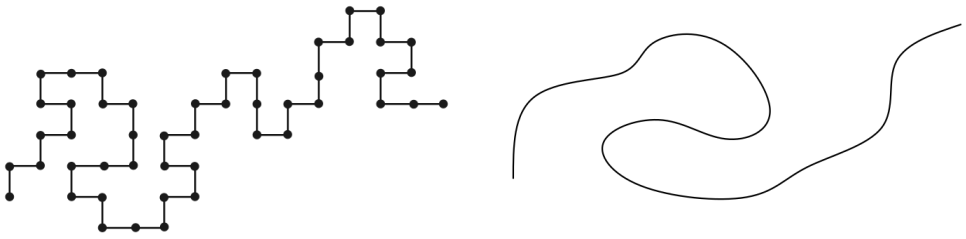

(a) (b)

Figure 1.2: **(a)** A sequence of monomers joined by edges is a discrete polymer walk (chain). In this figure we can see a walk in a square lattice (2 dimensions). **(b)** If we take the distance between monomers in a walk to zero, keeping the density constant, we get the continuous limit of a walk. It is often convenient, even when thinking about discrete walks, to represent polymers this way when talking about topology proprieties or depicting configurations. We are going to do so.

Walks Let us begin with a generic polymer walk (chain) (figure 1.2), made of N monomers, in some lattice in $\mathbb{R}^d$: it can present itself in a number of different configurations.
Let us consider all and only the self avoiding ones.
A polymer chain is a critical system. This was recognized by De Gennes in [3] by showing how one can establish a map between this system and a magnetic n-components spin model, with $O(n)$ symmetry, in the limit $n \to 0$. This is achieved by first associating (bijectively) each term of the partition function of the $O(n)$ model on a given lattice with a diagram representing a walk on the same lattice and then sending $n \to 0$ in order to eliminate the not self-avoiding ones.
This made it possible to calculate the size and configuration exponents γ and ν such that

$$\mathscr{Z}_N \sim \mu^N N^{\gamma-1} \qquad (N \gg 1) \tag{1.1}$$

$$\langle R^2 \rangle \sim N^{2\nu} \qquad (N \gg 1), \tag{1.2}$$

where $\langle R^2 \rangle$ is the averaged[1] squared end-to-end distance and $\mathscr{Z}_N$ is the configuration number, the number of walks in $\mathbb{R}^d$ made of N monomers. μ is the connectivity constant and depends on the model[2], while ν and γ are the analogous of the correlation length and susceptibility exponents of the magnetic model. If we denote $d = 4 - \epsilon$ then, using field theory, one can expand ν and γ in powers of ϵ (e.g. [4]). Up to third order[3]

$$\nu = \frac{1}{2}\left\{1 + \frac{\epsilon}{8} + \frac{15}{4}\left(\frac{\epsilon}{8}\right)^2 + \left[\frac{135}{8} - 33\xi(3)\right]\left(\frac{\epsilon}{8}\right)^3 + \mathcal{O}(\epsilon^4)\right\} \tag{1.3}$$

$$\gamma = 1 + \frac{\epsilon}{8} + \frac{13}{4}\left(\frac{\epsilon}{8}\right)^2 + \left[\frac{97}{8} - 33\xi(3)\right]\left(\frac{\epsilon}{8}\right)^3 + \mathcal{O}(\epsilon^4). \tag{1.4}$$

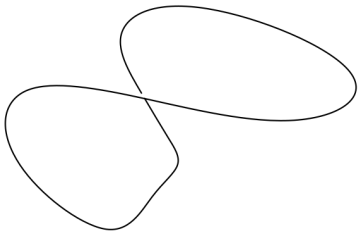

Figure 1.3: A polymer loop is a polymer walk with coinciding starting and ending monomers. In this figure we can admire an unknotted loop (in $\mathbb{R}^3$), symbolized by $\emptyset$, in 3 dimensions: it can be continuously deformed to a circle S^1.

Loops A particular type of polymer walk are loops, i.e. closed chains.
Using again de Guennes equivalence, considering self-avoiding loops in the cubic lattice ($\mathbb{Z}^3$) without topology constrains and made of N monomers, the following not rigorous but strongly supported asymptotic behavior is suggested[4]

$$\mathscr{Z}_N = A N^{\alpha-1} \mu^N \left(1 + \frac{B}{N^\Delta} + \frac{C}{N} + \dots\right) \qquad (N \gg 1) \tag{1.5}$$

[1] On all the configurations with fixed N.

[2] That usually means lattice type.

[3] $\xi(t) = \sum_{n=1}^{\infty} \frac{1}{t^n}$, $\Re(t) > 1$ is the Riemann's function. $\xi(3) \approx 1.202$.

[4] This is generally accepted as the correct approximation. Note that we use α and β as names of the critical exponent to distinguish them from γ and ν

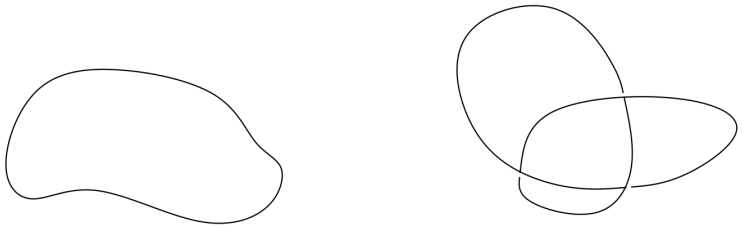

(a) (b)

Figure 1.4: In 3 dimensions, not every couple of loops can be mapped one into the other with continuous transformations. Hence, we group configurations among knot type classes. **(a)** This is an example of unknotted loop ø. **(b)** This configuration can't be deformed into a circle, so it belongs to a different class than the unknotted one. We are observing a trefoil knot, labeled 3_1 (3 is the number of crossings, 1 is a subscript to identify this particular type between all the ones with 3 crossings).

$$\langle R^2 \rangle = A_\beta N^{2\beta} \left(1 + \frac{B_\beta}{N^\Delta} + \frac{C_\beta}{N} + \dots \right) \qquad (N \gg 1). \tag{1.6}$$

This time, $\langle R^2 \rangle$ can't be an end to end mean distance: it is the average of the squared radius of gyration, $R^2 = \frac{1}{N} \sum_{i=1}^{N} (\vec{r}_i - \langle \vec{r}_i \rangle)^2$, where $\vec{r}_i$ are the positions of the monomers of a configuration and $\langle \vec{r}_i \rangle$ their mean value. Here, μ, α, β and Δ are deemed to be lattice independent and their best estimates are: $\mu = 4.68393 \pm 0.00002$ [5], $\alpha = -1.763 \pm 0.004$ [6], $\beta = 0.5882 \pm 0.0010$ and $\Delta = 0.475 \pm 0.0010$ [7]. A, B, C and A_β, B_β, C_β are some coefficients and the index β is only used to distinguish the two sets.
A topology property of loops in 3 dimensions is that we can't always map one configuration into another without breaking it, as we can see in figure 1.4. Equivalence classes thus generated are called knot types.
Can something be said for $\mathscr{Z}_N$ with a fixed topology (i.e. knot type)?
Let us indicate with τ a given knot type. Soteros *et al* [8] demonstrated that

$$\lim_{N\to\infty} \inf \frac{\ln \mathscr{Z}_N(\tau)}{N} = k_\tau \leq \lim_{N\to\infty} \sup \frac{\ln \mathscr{Z}_N(\tau)}{N} = K_\tau \leq \lim_{N\to\infty} \frac{\ln \mathscr{Z}_N}{N} = k, \tag{1.7}$$

with $0 < k < \infty$ (Hammersley [9]).
Only for the unknotted type is known that $k_\tau = K_\tau$; nevertheless, $\ln \mathscr{Z}_N(\tau)$ will

grow exponentially with N and[5] $DN^{\frac{2}{3}} \leq \langle R_N^2(\tau)\rangle \leq N^2$, for some $D > 0$. Consequentely it seems reasonable to assume that[6]

$$\mathscr{Z}_N(\tau) = A(\tau)N^{\alpha(\tau)-1}\mu(\tau)^N\left(1 + \frac{B(\tau)}{N^{\Delta(\tau)}} + \dots\right) \qquad (N \gg 1) \qquad (1.8)$$

$$\langle R^2(\tau)\rangle = A_\beta(\tau)N^{2\beta(\tau)}\left(1 + \frac{B_\beta(\tau)}{N^{\Delta(\tau)}} + \frac{C_\beta(\tau)}{N} + \dots\right) \qquad (N \gg 1). \qquad (1.9)$$

Note that there are evidence (e.g. [1]), that approximations of the sort $\mu(\tau) \approx \mu$ and $\alpha(\emptyset) \approx \alpha$ hold true up to the fifth and second decimal place rispectively.
Finally, another interesting result that will be of use in this work is to be find in Orlandini *et al* [1].
If we are dealing with a knotted polymer loop and assume that the region of the knot is localized, with a $o(N)$ size[7], then, for $N \gg 1$, we can treat the knot as a point: it contributes with a factor N (i.e. the number of possible position of this point on the polymer) to $\mathscr{Z}_N(\tau)$, so that $\alpha(\tau) = \alpha(\emptyset) + 1$.

In the attempt to extrapolate what we know for one loop to the Hopf link, the questions we are addressing are:

1. what happens, in the asymptotic limit, to the number of configurations $\mathscr{Z}$ if we consider a couple of linked polymer loops instead of one? Can we still find a connectivity constant μ and an exponent γ such that $\mathscr{Z}_N \sim N^{\gamma-1}\mu^N$ for $N \gg 1$, where N is the total length (i.e. total number of monomers) of the link?

2. Can we say some configurations are favored more than others?

As we stated in the previous paragraph, there are encouraging results leading towards the possibility of localized knots on loops to behave like points.
As a result, an idea that can perhaps give us some information is to be find in Duplantier's work on polymer networks [2].
Imagine that the region in which two polymers are linked is localized; then, for large lengths, we can establish a connection between this system and a network made of two branches and a single 4-legged vertex, the eight-like network, as we can see in figure 1.5. From Duplantier's results, one can expect a network $\mathcal{G}$ composed of branches of the same length N, with fixed topology (only that of the vertices: the topology of the branches is free to vary, i.e. the branches can be knotted), to scale like $\mathscr{Z}_N \sim \mu^N N^{\gamma_\mathcal{G}-1}$, $\gamma_\mathcal{G}$ being a topology dependent exponent

[5] Remember that we are considering only self-avoiding configurations.
[6] For some results that support this assumption see [1].
[7] It can be $\sim \log(N)$, N^{-1}, etc.

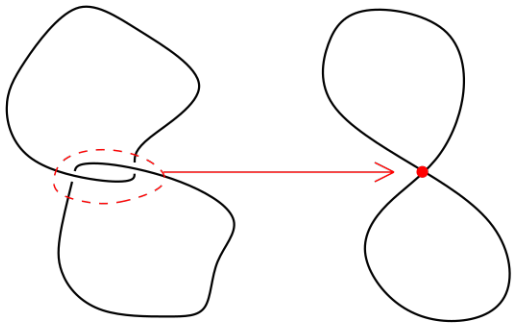

Figure 1.5: If the link region of the Hopf link becomes a point, we get an unknotted network with a node and two branches. It has a shape of an 8, so we are calling it eight-like network.

that can be calculated approximately in 3 dimensions. What we want to do is make a comparison between this formula and a simulative calculation of $\mathscr{Z}_N$ for the Hopf link, in order to test if, indeed, in the asymptotic large lengths limit, we can say that the configurations in which the linked region becomes a point ($o(N)$ small) are predominant or not.
This work is organized as follows:

- In chapters 2 and 3 we will first illustrate how in direct renormalization theory, factorizing over the branches and the vertices, Douplantier obtained the announced scaling behavior. Then, using the insight gained from that, we will proceed to associate, to some degree of approximation to be stated, an exponent γ to certain asymptotic configuration types with the Hopf topology.

- After that, we are going to set up a computational simulation. In chapter 4 we will illustrate how we extended the BFACF[8] algorithm for polymer loops on the cubic lattice to links and, in chapter 5, we will show that the ergodicity classes of the new algorithm are link types.

- Finally, in chapter 6 we are going to illustrate our computational results and compare them with the theory of chapter 3.

[8]Berg-Foerster-Aragao de Carvalho-Caracciolo-Frohlich.

Chapter 2

Statistical Mechanics of Polymer Networks

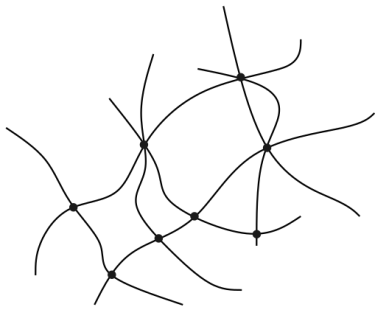

Figure 2.1: A polymer network is an object made of a set of points called vertices and lines called branches connecting them. In this example, we can see a network with 8 vertices of various multiplicity, which is the number of branches attached to them.

2.1 Decomposition of a network: star polymers

As we stated in chapter 1, we want to describe the asymptotic behavior of the Hopf link by associating it with that of polymer networks (figure 2.1). Understanding Duplantier's theory is hence necessary and will be the topic of this chapter.

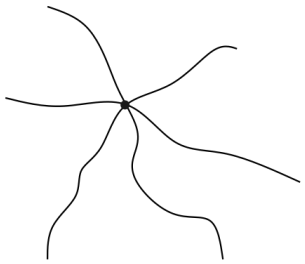

Figure 2.2: A vertex and L polymer chains attached to it is what we call an L-legged star polymer. In this figure we can see a 6-legged star polymer.

Star polymers We will see that the basic idea to deal with a network is to factorize its partition function over its vertices, or to better say over the star polymers (figure 2.2) made by the vertices and their attached branches.
Let $\mathscr{S}_L$ be a star with L legs all made of N monomers. Its number of self-avoiding configurations [10] is a generalization of 1.1:

$$\mathscr{Z}_N(\mathscr{S}_L) \sim \mu^{LN} N^{\gamma_L - 1} \qquad (N \gg 1). \tag{2.1}$$

- For $L = 1$ we have a single chain, so $\gamma_1 = \gamma$;
- for $L = 2$ we have the same as above, so $\gamma_2 = \gamma$;
- for $L \geq 3$, γ_L are a new set of independent critical exponents to be determined.

When studying star polymers and chains also other exponents are of interest. All of these can be unified in a single infinite but numerable set of independent and universal critical exponents [10] σ_L, with $L \geq 1$ and integer. An example of this is

$$\gamma_L - 1 = \sigma_L + L\sigma_1 : \tag{2.2}$$

here the central vertex of the L-legged star polymers contributes with σ_L, while the L branches with σ_1 each.
This statement means that a star polymer depends only on the number of its legs, so that what really matter is the vertex.

Let now $\mathscr{G}$ be a polymer network, made of $\mathscr{N}$ chains of equal length N, in $d = 4 - \epsilon$ dimensions. We call vertex topology of $\mathscr{G}$ the number of its vertices and

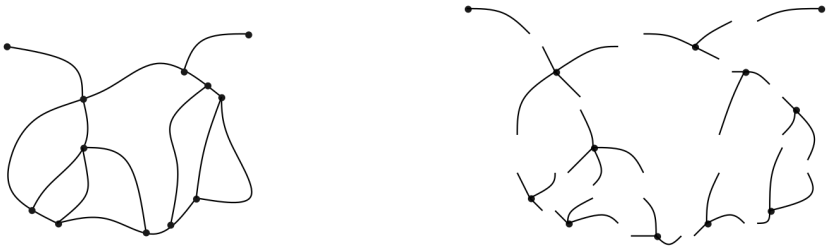

Figure 2.3: The decomposition of a polymer network $\mathscr{G}$ of fixed but arbitrary vertex topology. In this example, we have $n_1 = 2$, $n_3 = 8$ and $n_4 = 2$. The number of independent loops, by Euler's formula, is $1 - 1 + 4 + 2 = 6$, as we can somehow tell directly from the figure.

the way they are connected to each other through the branches. Let us assume that $\mathscr{G}$ has arbitrary but fixed vertex topology[1]. Duplantier argued [3] that: if we call n_L the number of vertices of functionality L, $L \geq 1$, the asymptotic number of self-avoiding configurations of $\mathscr{G}$ is

$$\mathscr{Z}_N(\mathscr{G}) \sim \mu^{\mathscr{N}N} N^{\gamma_{\mathscr{G}}-1} \qquad (N \gg 1), \tag{2.3}$$

where $\gamma_{\mathscr{G}}$ is the topology dependent critical exponent[2]

$$\gamma_{\mathscr{G}} - 1 = -\nu d\mathscr{L} + \sum_{L\geq 1} n_L \sigma_L \tag{2.4}$$

and $\mathscr{L}$ is the number of physical loops in the network $\mathscr{G}$, given by Euler's formula

$$\mathscr{L} = 1 + \frac{1}{2}\sum_{L\geq 1} n_L(L-2). \tag{2.5}$$

Note that $\sigma_2 = 0$ is a necessary condition, since every single point of a branch can be interpreted as a 2-legged star polymer, so that $n_2 = \infty$. In [3], one can also find an estimate of σ_L as a series of powers of ϵ up to second order:

$$\sigma_L = \left(\frac{\epsilon}{8}\right)(2-L)\frac{L}{2} + \left(\frac{\epsilon}{8}\right)^2(L-2)(8L-21)\frac{L}{8} + \mathcal{O}(\epsilon^3). \tag{2.6}$$

In the next section, we are going to illustrate how one can obtain these results.

[1] Note that we are not fixing how the branches are structured: they can be knotted or linked to each other.

[2] ν is the same as above.

2.2 Partition function of the continuous model

Let $\mathscr{G}$ be a self-avoiding polymer network made of $\mathscr{N}$ independent polymer chains tied together in $\mathscr{V}$ vertices in $\mathbb{R}^d$, all but one (to remove translation invariance) without fixed positions, as long as the vertex topology of $\mathscr{G}$ is fixed.
We need to describe the system in its continuum limit.
In this limit, instead of the coordinates of all the monomers of every chains, we describe each branch with a curve in the ambient space, $\vec{r}_a(s)$. Here, s is a coordinate, with the dimension of an area, that is said to go from 0, at the start of the chain to $0 < S < \infty$, at its end, so it also conveys a purely conventional[3] orientation to the branches (figure 2.4). We are assuming that all the chains are of the same length: S is proportional to the number of monomers in the continuous limit $N \to \infty$, $l^d N \to S < \infty$, where $l \to 0$ would be the (fixed) distance between them. Since in the continuous limit it represents the probability weight of all the configurations with a fixed number of monomers, our end goal is to factorize the partition function with fixed S over the vertices. The partition function of this model is a functional of all the $\mathscr{N}$ $\vec{r}_a(s)$; it is given by the standard Edwards continuum action [11]

$$\mathscr{Z}(\mathscr{G}) = \frac{\int \prod_{a=1}^{\mathscr{N}} d\{\vec{r}_a\} \delta^d[\mathscr{G}] \mathscr{P}_{\mathscr{N}}\{\vec{r}_a\}}{\Big[\int d\{\vec{r}\} P_0\{\vec{r}\} \delta^d(\vec{r}(0))\Big]^{\mathscr{N}}}, \tag{2.7}$$

with

$$\begin{aligned}
\mathscr{P}_{\mathscr{N}}\{\vec{r}_a\} = \exp\Bigg[&- \frac{1}{2} \sum_{a=1}^{\mathscr{N}} \int_0^S \left(\frac{d\vec{r}_a(s)}{ds} \right)^2 ds \\
&- \frac{1}{2} b \sum_{a=1}^{\mathscr{N}} \sum_{a'=1}^{\mathscr{N}} \int_0^S ds \int_0^S ds' \delta^d(\vec{r}_a(s) - \vec{r}_{a'}(s')) \Bigg] \\
\delta^d[\mathscr{G}] = \int \prod_{i=1}^{\mathscr{V}-1} d^d \vec{R}_i \prod_{i=1}^{\mathscr{V}} \Bigg[&\prod_{a \in L^+(i)} \delta^d(\vec{r}_a(0) - \vec{R}_i) \prod_{a' \in L^-(i)} \delta^d(\vec{r}_{a'}(S) - \vec{R}_i) \Bigg].
\end{aligned}$$

In $\mathscr{P}_{\mathscr{N}}$, the argument of the exponential is the sum of a kinetic term and a repulsive contact interaction. If only self-avoiding configurations are allowed, we need to send the interaction parameter b to ∞: in this way, whenever in the functional integral $\int \prod_{a=1}^{\mathscr{N}} d\{\vec{r}_a\}$ a configuration with auto-intersections is chosen,

[3] Edwards partition function does not depend on the orientation of the branches. It is important to remember that we are going to consider links without orientation or frame.

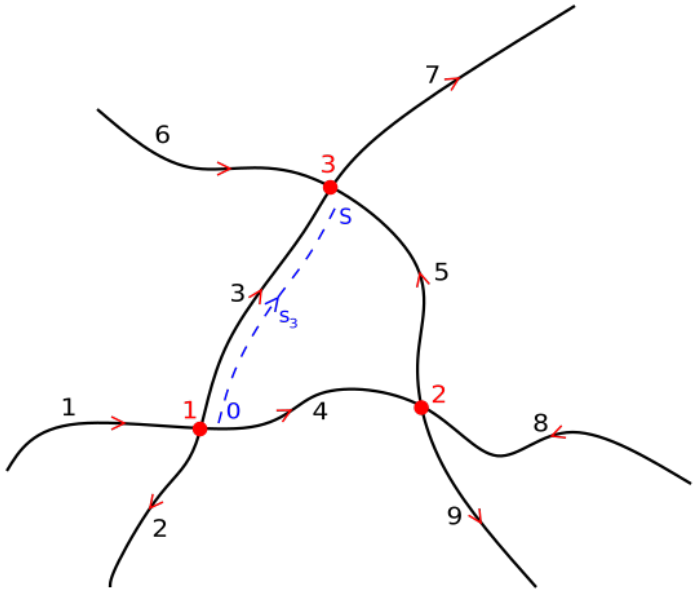

Figure 2.4: The parameter $s \in [0, S]$ conveys a conventional orientation to the curve representing the a-th branch, $\vec{r}_a(s)$, $a = 1, \ldots, \mathscr{N}$. We call $L^+(i)$ and $L^-(i)$, respectively, the collection of the indices of the chains going in and out from vertex i. In this example, $L^+(1) = \{1\}$, $L^-(1) = \{2, 3, 4\}$, $L^+(2) = \{4, 8\}$, $L^-(2) = \{5, 9\}$, $L^+(3) = \{3, 5, 6\}$ and $L^-(3) = \{7\}$.

the contact term diverges and $\mathscr{P}_{\mathscr{N}}\{\vec{r}_a\}$ goes to 0. $\delta^d[\mathscr{G}]$ fixes the vertex topology; $\vec{R}_i$, $i = 1, \ldots, \mathscr{V}$ are the positions of the $\mathscr{V}$ vertices, only $\mathscr{V} - 1$ of which are integrated in $\mathbb{R}^d$: one is fixed in order to remove translation invariance, and $L^+(i)$ and $L^-(i)$ are, respectively, the collection of the indices of the branches going in and out from vertex i (figure 2.4). Moreover, $\mathscr{P}_0$ is the Brownian partition function ($b = 0$ and $\mathscr{N} = 1$): $\mathscr{Z}(\mathscr{G})$ is divided by the Brownian weight of its branches in order to have a well defined continuous limit [11].

Ultraviolet cut-off The contact interaction in expression 2.7 yields a divergent contribution when $s = s'$ (see appendix A). The way to bypass this problem is to introduce a short-distance ultraviolet cutoff, $|s - s'| \geq s_0$ in the limit $s_0 \to 0$, and go on with the calculations. By doing this we are introducing s_0, a new parameter, in $\mathscr{Z}$; but in the limit $s_0 \to 0$ and for $d < 4$, it is possible to factorize it out [12]:

$$\underset{s_0 \to 0}{\mathscr{Z}}(\mathscr{G}, b, S, s_0, d) = \exp[\mathscr{N}(S/s_0)C(z_0)]\mathscr{Z}(\mathscr{G}, b, S, d)|_{dim.reg.}. \tag{2.8}$$

z_0 is the cut-off dependent and dimensionless interaction parameter

$$z_0 = (2\pi)^{-\frac{d}{2}} b s_0^{2-\frac{d}{2}}, \tag{2.9}$$

$C(z_0)$ is a regular function [12] of z_0 independent of $\mathscr{G}$ and $\mathscr{Z}(\mathscr{G})|_{dim.reg.}$ is the dimensional regularized [13] partition function[4], which will depend [12] on S and on the dimensionless interaction parameter

$$z = (2\pi)^{-\frac{d}{2}} b S^{2-\frac{d}{2}}. \tag{2.10}$$

Given that we can interpret $\mathscr{N}(S/s_0)$ as a sort of number of monomers of our continuous model, we have extracted the "$\mu^{\mathscr{N}N}$ part" of $\mathscr{Z}$, with $\mu = e^{C(z_0)}$. Now we need to show that

$$\mathscr{Z}(\mathscr{G}, b, S, d)|_{dim.reg.} \sim S^{\gamma_{\mathscr{G}}-1} \qquad (S \to \infty). \tag{2.11}$$

From now on, we will work in dimensional regularization (i.e. $\mu = 1$).

2.3 Asymptotic limit and renormalization

If we want to reach an universal scaling behavior, we have to perform the asymptotic limit in an appropriate way.

Renormalization of polymer chains For a self-avoiding polymer chain, the asymptotic limit is reached by increasing the number of monomers, namely[5] $z \to \infty$, $S \to \infty$, while performing a scaling transformation so to preserve the mean end to end distance.
Hence, we need a new scale to express quantities.
If R^2 is the mean squared end to end distance, namely

$$R^2 = \langle [\vec{r}(S) - \vec{r}(0)]^2 \rangle, \tag{2.12}$$

it can be shown [12] that, for the Edwards model and $d = 4 - \epsilon$,

$$\begin{aligned} R^2 &= \mathscr{H}_0(z, d) dS \\ \mathscr{H}_0(z, d) &\to A_0(\epsilon) z^{(2\nu-1)\frac{2}{\epsilon}} \qquad z \to \infty, \end{aligned} \tag{2.13}$$

where $A_0(\epsilon)$ is an amplitude and ν is the correlation length exponent[6] 1.3. $\mathscr{H}_0$ is called swelling factor and, given that we want to preserve R^2, if we multiply it by S, we get the scale we were searching for.
We shall apply this to the self-avoiding networks.

[4] Meaning that it is free of ultraviolet divergences. It is obtained continuing analytically the model for $d < 2$, which is free of this problem.

[5] Note that we are assuming $d < 4$.

[6] Remembering the definition of z, we get $R^2 \sim S^{2\nu}$, like we would expect.

Dimensional analysis Now that we have an appropriate scale, by a simple dimensional analysis we can factorize out of the partition function the hyperscaling contribution of the loops of a given network topology.
We can achieve this by first extracting the scaling in S of the partition function by checking its physical dimension, and then plugging in the expression of S in terms of the physical scale.
Given that the dimensional contribution of each δ^d in $\delta^d[\mathscr{G}]$ is, remembering that S is an area, $S^{-\frac{d}{2}}$:

$$\delta(r_a(s)) = \delta\Big(\sqrt{S}\frac{r_a(s)}{\sqrt{S}}\Big) = \frac{1}{\sqrt{S}}\delta(r'_a(s)),$$

with $r'_a(s) = \frac{r_a(s)}{\sqrt{S}}$ dimensionless; the contribution of $\delta^d[\mathscr{G}]$ is

$$\delta^d[\mathscr{G}] \sim S^{-\Delta\frac{d}{2}}, \tag{2.14}$$

with

$$\Delta = \sum_{i=1}^{\mathscr{V}} (L^+(i) + L^-(i)) - (\mathscr{V} - 1).$$

Note that the subtraction of $\mathscr{V}-1$ is due to the integration over the position of (all but one) the vertices. Taking also into account the contribution of each integral over $\vec{r}_a(s)$, we have

$$\begin{aligned} \mathscr{Z}(\mathscr{G}) &= (2\pi S)^{(\mathscr{N}-\Delta)\frac{d}{2}} Z(\mathscr{G}, z, d) \\ &= (2\pi S)^{-\mathscr{L}\frac{d}{2}} Z(\mathscr{Z}, z, d), \end{aligned} \tag{2.15}$$

$\mathscr{L}$ is the Euler number 2.5 of independent loops and Z a dimensionless function (one can check that $\mathscr{N} - \Delta = -\mathscr{L}$).
Using the proper scale, we can now extract the hyperscaling contribution of the internal loops of a network topology

$$\begin{aligned} \mathscr{Z}(\mathscr{G}) &= (2\pi R^2/d)^{(\mathscr{N}-\Delta)\frac{d}{2}} Z_v(\mathscr{G}, z, d) \\ Z_v(\mathscr{G}, z, d) &= [\mathscr{H}_0(z, d)]^{\mathscr{L}\frac{d}{2}} Z(\mathscr{G}, z, d). \end{aligned} \tag{2.16}$$

Factorization over the vertices What remains is the contribution of the vertices, stored in Z_v.
The idea is that the divergences come from the core of the vertices (figure 2.5), so we want to factorize Z_v in terms of the reduced partition function of the L-legged star polymers ($\mathscr{S}_L$)

$$\begin{aligned} \hat{Z}_L(z, d) &= \mathscr{Z}(\mathscr{S}_L)[\mathscr{Z}(\mathscr{S}_1)]^{-\frac{L}{2}} \\ &= Z(\mathscr{S}_L, z, d)[Z(\mathscr{S}_1, z, d)]^{-\frac{L}{2}}, \end{aligned} \tag{2.17}$$

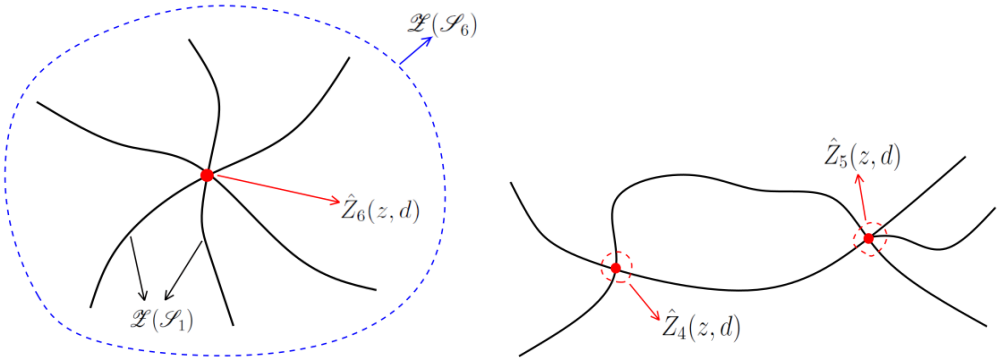

(a) (b)

Figure 2.5: **(a)** The divergences come from the *cores* of the star polymers composing a network topology: we need to normalize the partition function, $\mathscr{Z}(\mathscr{S}_L)$, of an L-legged star polymer by the product of these of its branches, $[\mathscr{Z}(\mathscr{S}_1)]^L$. **(b)** In this way, in the decomposition of the partition function, we associate a contribution $\hat{Z}_L(z,d) = \mathscr{Z}(\mathscr{S}_L)[\mathscr{Z}(\mathscr{S}_1)]^{-\frac{L}{2}}$ to each vertex with L chains connected.

where the division by $\mathscr{Z}(\mathscr{S}_1)$ is done to isolate the cores from the L branches[7]. We can always rewrite the partition function of a general network (topology) $\mathscr{G}$, with n_L vertices of L legs, $L \geq 1$, as

$$\mathscr{Z}(\mathscr{G}, b, S, d) = [2\pi S \mathscr{H}_0(z,d)]^{-\mathscr{L}\frac{d}{2}} \prod_{L\geq 1} [\hat{Z}_L(z,d)]^{n_L} \mathscr{A}(\mathscr{G}, z, d) \tag{2.18}$$

where $\mathscr{A}(\mathscr{G}, z, d)$ is a dimensionless function of z and d.
This last step is just a matter of definitions, the following assumption is the essence of the problem [2].

Proposition 2.1. *Any scaling behavior in power of S has been factorized out. Hence, the residual amplitude $\mathscr{A}(\mathscr{G}, z, d)$ reaches a finite fixed point value in the asymptotic limit $z \to \infty$ or $S \to \infty$:*

$$\mathscr{A}(\mathscr{G}, z, d) \to \mathscr{A}^*(\mathscr{G}, \infty, d) < \infty \tag{2.19}$$

This statement is a nontrivial one [2], it means that we can completely factorize the divergences of the partition function of a network $\mathscr{G}$ over its internal loops and vertices.

[7] The second equivalence comes from $\mathscr{L}(\mathscr{S}_1) = 1$.

Critical exponents The last thing remaining to obtain the announced asymptotic behavior is to plug in the factorization 2.18 the scaling law of polymer stars. We know, from what we learned in section 2.1, that

$$\mathscr{Z}(\mathscr{S}_L) \underset{z\to\infty}{=} A_L(\epsilon) z^{(\gamma_L-1)\frac{2}{\epsilon}} \sim S^{\gamma_L-1}, \tag{2.20}$$

where $A_L(\epsilon)$ is a calculable amplitude. The reduced partition function reads

$$\hat{Z}_L(z,\epsilon) \underset{z\to\infty}{=} \hat{A}_L(\epsilon) z^{\sigma_L\frac{2}{\epsilon}} \sim S^{\sigma_L}, \tag{2.21}$$

where σ_L is a new set (for $L \geq 1$) of universal independent exponents we mentioned earlier

$$\sigma_L = \gamma_L - 1 - \frac{1}{2}(\gamma - 1) \tag{2.22}$$

γ is the same of equation 1.4 and $\hat{A}_L = A_L A_1^{-\frac{L}{2}}$. Thus, combining all these expressions, remembering the scaling 2.13 of the swelling factor, we get

$$\mathscr{Z}(\mathscr{G}) \underset{\substack{z\to\infty \\ S\to\infty}}{=} [2\pi S A_0(\epsilon) z^{(2\nu-1)\frac{2}{\epsilon}}]^{-d\frac{\mathscr{L}}{2}} \prod_{L\geq 1} [\hat{A}_L(\epsilon) z^{\sigma_L\frac{2}{\epsilon}}]^{n_L} \mathscr{A}^*(\mathscr{G}). \tag{2.23}$$

In terms of S, we have

$$\mathscr{Z}(\mathscr{G}) \sim S^{-\nu d\mathscr{L} + \sum_{L\geq 1} n_L \sigma_L} \qquad S \to \infty, \tag{2.24}$$

giving

$$\gamma_{\mathscr{G}} - 1 = -\nu d\mathscr{L} + \sum_{L\geq 1} n_L \sigma_L. \tag{2.13}$$

The only thing left is to actually compute the exponents σ_L. In order to do that, we need to perform a perturbative expansion of $\hat{Z}_L(z,d)$

Perturbation expansion and coefficients σ_L A dimensionless partition function, Z, admits a double Laurent-Taylor expansion in z and ϵ as follows

$$\begin{aligned} \frac{Z(\mathscr{G},z,d)}{Z^B(\mathscr{G},d)} &= 1 + \sum_{n\geq 1} a_n(\epsilon) z^n \\ a_n(\epsilon) &= \frac{\alpha_{n,n}}{\epsilon^n} + \frac{\alpha_{n,n-1}}{\epsilon^{n-1}} + \cdots + \alpha_0(\epsilon), \end{aligned} \tag{2.25}$$

with $\alpha_0(\epsilon)$ regular for $\epsilon \to 0$ and $\mathscr{Z}^B$ being the Brownian partition function.
To obtain this, one has to expand $\mathscr{P}_{\mathscr{N}}$ in expression 2.7 in power of b and regularize the divergences. The rules to perform this type of calculations for any given network topology $\mathscr{G}$, as well our first order calculations for the specific networks

we will be using can be found in appendix A.

With this knowledge, the basic method for obtaining σ_L in $d = 4 - \epsilon$ is to first calculate the perturbative expansion of $\hat{Z}_L(z, d)$ and than take the limit $z \to \infty$ of the scaling functions

$$\sigma_L(z, \epsilon) = S\frac{\partial}{\partial S} \ln \hat{Z}_L(z, d). \tag{2.26}$$

Their fixed point value yields the critical exponents and is obtained (renormalizing) by substituting z in the previous expression with the fixed point of the dimensionless second virial coefficient, g [2] [12], namely, to second order

$$g(z \to \infty, \epsilon) = g^*(\epsilon) = \frac{\epsilon}{8} + \left(\frac{\epsilon}{8}\right)^2 \left(\frac{25}{4} + 4 \ln 2 + \dots\right) \tag{2.27}$$

We then find, up to second order[8],

$$\sigma_L(z \to \infty, \epsilon) = \sigma_L[g^*, \epsilon] \tag{2.28}$$

$$\sigma_L = \left(\frac{\epsilon}{8}\right)(2 - L)\frac{L}{2} + \left(\frac{\epsilon}{8}\right)^2 (L - 2)(8L - 21)\frac{L}{8} + \mathcal{O}(\epsilon^3). \tag{2.6}$$

Lastly, note that one can also calculate the amplitude $\mathscr{A}^*(\mathscr{G}, d)$, so to obtain the complete asymptotic limit[9] (up to some order) in a similar way: if the expansion of $\mathscr{Z}(\mathscr{G})$ is known, one can invert equation 2.18 by using the expansions of $\mathscr{H}_0(z, d)$ and $\hat{Z}_L(z, d)$ and replace z with g^*.

[8] For $d > 4$ the scaling behavior is trivial, hence $\sigma_L \equiv 0$.

[9] $A_0(\epsilon)$ and $\hat{A}_L(\epsilon)$ are known.

Chapter 3

Asymptotic Behavior of Two Linked Loops

Let us call $N = N_1 + N_2$ the sum of the lengths of two linked loops and assume that, in the $N \to \infty$ limit, $N_1 = \mathcal{O}(N)$ and $N_2 = \mathcal{O}(N)$. By defining a characteristic length l for the linked portion, e.g. taking the radius of the smallest sphere that contains it, like illustrated in figure 3.1, two possible situations can arise in the large N limit: $l = o(N)$ or $l = \mathcal{O}(N)$.
In the next section, we will try to quantify, in the $l = o(N)$ case, the asymptotic

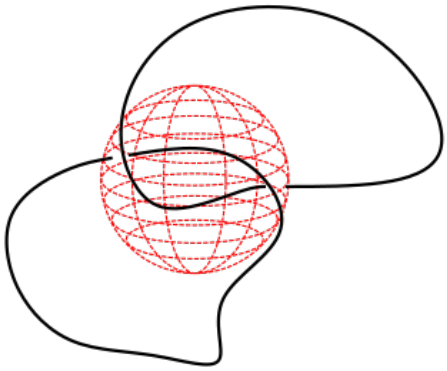

Figure 3.1: As illustrated in this figure, we can define the characteristic length of the linked portion of two linked loops as the radius of the smallest sphere that contains the linked region, if we can identify it.

behavior of links with the Hopf topology, $\mathscr{H}$, by identifying a correspondent network topology. We will assume that the number of Hopf configurations (links) with

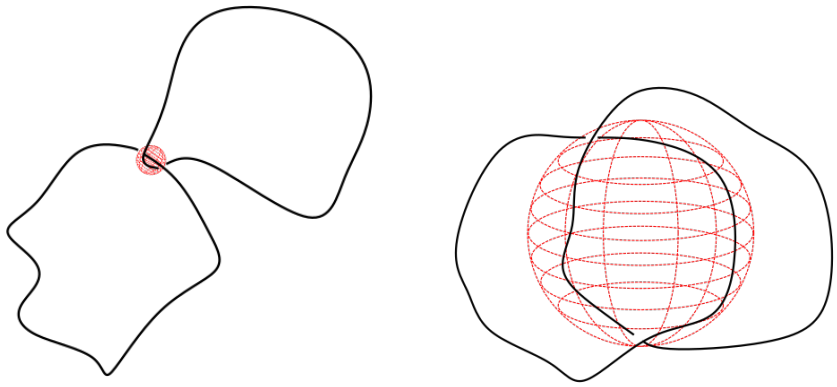

(a) (b)

Figure 3.2: **(a)** In the large N limit for two linked loops forming an Hopf link with total length N, two possible situations can arise: the linked portion can have a characteristic length $l = o(N)$ or **(b)** $l = \mathcal{O}(N)$.

total length N scales, in the large N limit, in the way as the partition function of monodisperse networks[1]:

$$\mathscr{Z}_N(\mathscr{H}) \sim \mu^N N^{\gamma_{\mathscr{H}}-1} \qquad (N \gg 1), \tag{3.1}$$

and we will estimate the exponent $\gamma_{\mathscr{H}}$ as the correspondent network one.
In section 3.2, we are going to do the same in the $l = \mathcal{O}(N)$ case.

3.1 Localized linked portion

If $l = o(N)$, we say that the linked portion is localized and, in the asymptotic limit $N \to \infty$, the linked region itself becomes a point, so that the Hopf configurations can be described as networks with the eight-like topology, $\mathscr{G}_1$, as one can see in figure 3.3. Note that this consideration holds true only if the two loops of the links grow in the same way, $\mathcal{O}(N)$, in the large N limit.
The polydisperse case also falls under this category: if we suppose that one of the two loops grows as $o(N)$, then, in the asymptotic limit, we get single unknotted loops with a point that includes the linked portion, like shown in figure 3.4.
By using the theory of chapters 1 and 2, we will now compute $\gamma_{\mathscr{H}}$ in the localized case, extracting its value from that of the exponent $\gamma_{\mathscr{G}_1}$ of the eight-like networks ($\gamma_{\theta+p}$ of loops with a point).

[1]Here, the conditions $N_1 = \mathcal{O}(N)$ and $N_2 = \mathcal{O}(N)$ are required.

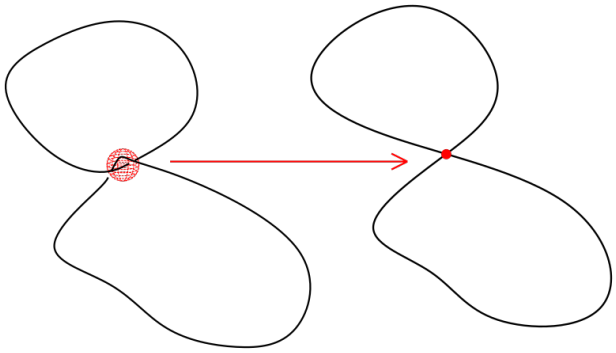

Figure 3.3: Network associated to two unknotted linked loop, in the asymptotic limit, in the case of localized linked region and monodisperse link. The linked portion becomes a point, so we get an eight-like network, made of a vertex of functionality 4 and 2 independent loops.

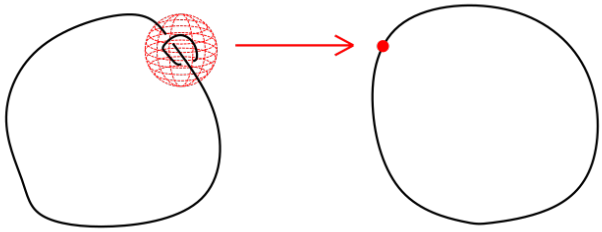

Figure 3.4: If we call N the total length of an Hopf link and suppose that one of the two loops grows as $o(N)$, then, in the asymptotic limit, we get an unknotted loop with a point.

3.1.1 Monodisperse link

Duplantier's formula Let us start from the monodisperse case.
In chapter 2 we understood that, for the monodisperse networks in $d = 4 - \epsilon$ dimensions made of $\mathscr{N}$ branches of N monomers each, n_L vertices with functionality $L \geq 1$ and $\mathscr{L}$ independent loops, we have:

$$\gamma_{\mathscr{G}} - 1 = -\nu d\mathscr{L} + \sum_{L\geq 1} n_L \sigma_L, \tag{2.4}$$

where, up to third and second order in ϵ respectively,

$$\nu = \frac{1}{2}\left\{1 + \frac{\epsilon}{8} + \frac{15}{4}\left(\frac{\epsilon}{8}\right)^2 + \left[\frac{135}{8} - 33\xi(3)\right]\left(\frac{\epsilon}{8}\right)^3 + \mathcal{O}(\epsilon^4)\right\} \tag{1.3}$$

$$\sigma_L = \left(\frac{\epsilon}{8}\right)(2-L)\frac{L}{2} + \left(\frac{\epsilon}{8}\right)^2 (L-2)(8L-21)\frac{L}{8} + \mathcal{O}(\epsilon^3). \tag{2.6}$$

For the eight-like networks, we have only one vertex with functionality 4 and in 3 dimensions $\epsilon = 1$.

- $\mathscr{L} = 2$.
  This is somehow clear from the picture, but one can also check it by using Euler's formula 2.5: $\mathscr{L} = 1 + \frac{1}{2}\sum_{L\geq 1} n_L(L-2) = 1 + \frac{1}{2}1(4-2) = 2$.
- $\nu \approx \frac{1}{2}\{1 + 0.125 + 0.059 - 0.044\} = 0.570$ and
- $\sigma_4 \approx -0.5 + 0.172 = -0.328$;

we then have

$$\gamma_{\mathscr{G}_1} \approx 1 - 3.420 - 0.328 = -2.748. \tag{3.2}$$

Additional configuration factor We can't straight up assume $\gamma_{\mathscr{H}} = \gamma_{\mathscr{G}_1}$.
It is important to note that even if the linked portion asymptotically becomes a point, two linked loops are not a network: they are not welded in a fixed point and the positions in which the loops are linked can change between configurations.
On the other hand, associating them with eight-like networks implies fixing a "link point", namely a point on both loops. Hence, to count the number of monodisperse Hopf links with localized linked region, we need to multiply the partition function of the eight-like networks by a factor $\sim N^2$. This procedure is illustrated in figure 3.5. The result is

$$\gamma_{\mathscr{H}} = \gamma_{\mathscr{G}_1} + 2 \approx -0.748. \tag{3.3}$$

We can also check this argument from Edwards partition function 2.7 itself.
In this function, the vertex topology of the networks counted is fixed by the integrand factor $\delta^d[\mathscr{G}]$. For the (monodisperse) eight-like topology it reads, if we call $\vec{r}_1(s)$ and $\vec{r}_2(s)$ the curves in $\mathbb{R}^3$ corresponding, in the continuous limit, to the two branches,

$$\delta^3[\mathscr{G}_1] = \delta(\vec{r}_1(0) - \vec{X})\delta(\vec{r}_1(S) - \vec{X})\delta(\vec{r}_2(0) - \vec{X})\delta(\vec{r}_2(S) - \vec{X}), \tag{3.4}$$

where $\vec{X}$ is the position of the vertex. If we were to write down a partition function for two self and mutual-avoiding loops with same length and a contact point, we would use the Edwards action with a $\delta^d[\mathscr{G}]$ factor of the form

$$\begin{aligned}\delta^3[\mathscr{G}'_1] = \int_0^S ds \int_0^S ds' \delta(\vec{r}_1(s) - \vec{X})\delta(\vec{r}_2(s') - \vec{X}) \\ \times\delta(\vec{r}_1(s-S) - \vec{X})\delta(\vec{r}_2(s'-S) - \vec{X}).\end{aligned} \tag{3.5}$$

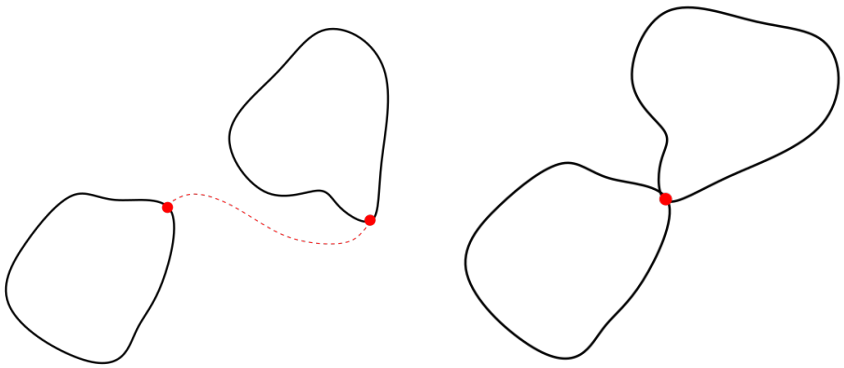

Figure 3.5: Even in the asymptotic limit, when the linked region becomes a point, two linked loops are not welded. The loops can be linked through any of their points, so we need to add a factor $\sim N^2$ to the partition function of the eight-like networks, when describing Hopf links.

If now, for every fixed value for s and s' of the integration region, we change the parameters so that $\vec{r}_1(s) \to \vec{r}_1(0)$ and $\vec{r}_2(s') \to \vec{r}_2(0)$, we get

$$\delta^3[\mathscr{G}'_1] = S^2\delta^3[\mathscr{G}_1]. \tag{3.6}$$

Loops topology An important issue to point out is that in Edwards partition function what is fixed is the vertex topology. What is free to vary in the physics described by it, is the topology of each branch. From figure 3.6, we see that for the eight-like networks, among all the possible configurations counted, there are not only ones with one or both branches turning around themselves and forming knots, but even ones with the branches interacting with each other forming links. If we used the scaling of the eight-like networks, and equation 3.3 as a consequence, to count the number of Hopf links (taking into account the factor mentioned in the previous paragraph), we would get an overestimate: there are no Hopf configurations corresponding to the ones pointed out. Even if we counted all the configurations obtained by letting the two loops of every Hopf link explore all their knot topologies, we would get an overestimate: to get link configurations corresponding to the eight-like ones with the branches linked to each other (figure 3.6(b)), we would need to cut open one of the loops and modify the topology.
In other words, we need to include a specific branching topology in the scaling law of the eight-like networks. We can find inspiration in the theory of knotted loops we gave a glimpse in chapter 1.

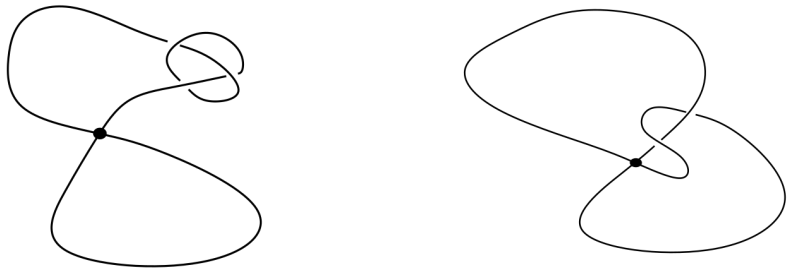

(a) (b)

Figure 3.6: Two eight-like networks counted in Edwards partition function: the vertex topology is fixed, but the branching one is free to vary.

We know that, for loops without fixed topology, the number of configurations reads, for large lengths N,

$$\mathscr{Z}_N = AN^{\alpha-1}\mu^N\left(1+\frac{B}{N^\Delta}+\frac{C}{N}+\dots\right) \qquad (N \gg 1), \tag{1.5}$$

whereas, if we fix a topology τ, it is usually assumed

$$\mathscr{Z}_N(\tau) = A(\tau)N^{\alpha(\tau)-1}\mu(\tau)^N\left(1+\frac{B(\tau)}{N^\Delta(\tau)}+\dots\right) \qquad (N \gg 1), \tag{1.8}$$

with $\mu(\tau) \approx \mu$ and $\alpha(\emptyset) \approx \alpha$ [15].
By analogy, we can assume, for the eight-like networks

$$\mathscr{Z}_N(\mathscr{G}_1(\tau)) \sim \mu(\tau)^N N^{\gamma_{\mathscr{G}_1(\tau)}-1} \qquad (N \gg 1), \tag{3.7}$$

where τ is a particular topology of the branches and, associating the Hopf topology of a link with the "unknotted" eight-like one of a network ($\mathscr{H} \leftrightarrow \mathscr{G}_1(\emptyset)$), remembering the additional configuration factor, $\mu(\mathscr{H}) \approx \mu$ and $\gamma_{\mathscr{H}} \approx \gamma_{\mathscr{G}_1} + 2$.
Our goal is to compute, through simulation, $\gamma_{\mathscr{H}}$ and compare it with the $\gamma_{\mathscr{G}_1}$ we estimated to see if they are compatible.
If we want to really associate the partition function of eight-like networks with a couple of linked loops, we have to take into consideration that in the configurations counted in Duplantier's power law, the two branches of the network can be linked one to another in any imaginable way. The only common feature of every one of these configurations is: both branches are $\mathcal{O}(N)$ near in at least one point , namely that represented by the vertex of the network. What we can state is that the scaling law of the eight-like networks (with the corrective factor mentioned

above) can be used to describe the asymptotic behavior of two linked loops with arbitrary topology but at least one contact point, a region in which the two loops are $o(N)$ near. We will concentrate on the Hopf topology, though.

3.1.2 Polydisperse link

We can predict, in a similar fashion, the asymptotic behavior of polydisperse Hopf configurations: in the large N limit these are associated to unknotted loops with a point.
Loops are a particular type of networks (indeed, the leading terms of the scaling of loops and the scaling law of networks have the same form) and remembering what we said previously, we can assume that

$$\mathscr{Z}_N(\mathscr{H}) \sim \mu^N N^{\gamma_{\emptyset+p}-1} \qquad (N \gg 1), \tag{3.8}$$

where $\emptyset + p$ is the topology of unknotted loops with a point.
We can find the value of $\gamma_\emptyset \equiv \alpha_\emptyset$ in chapter 1, the point adds an extra factor N to the number of configurations, so in this case we get

$$\gamma_{\mathscr{H}} = \gamma_{\emptyset+p} = \gamma_\emptyset + 1 = -0.763. \tag{3.9}$$

3.2 Delocalized linked portion

If $l = \mathcal{O}(N)$, we say that the linked portion is delocalized.
This case is more complicated, as associating a network with a link intuitively is justified when we are able to identify contact points (vertices) between the loops building the link, and for a general delocalized configuration this can't be done.
We can restrict ourselves to a particular case: if the delocalized linked region of an Hopf link can be described, in the asymptotic limit, by two separated contact points, then we can associate the link itself with a monodisperse network with the watermelon with 4 legs (all $\mathcal{O}(N)$) topology ($\mathscr{G}_2$). This is illustrated in figure 3.7. By the same arguments used in the previous section, we can now compute a value for the exponent $\gamma_{\mathscr{H}}$.

Duplantier's formula A watermelon network has 2 vertices with functionality 4 each and $\mathscr{L} = 3$: again, one can tell this from the picture, but also by checking Euler's formula: $\mathscr{L} = 1 + \frac{1}{2}\sum_{L\geq 1} n_L(L-2) = 1 + \frac{1}{2}2(4-2) = 3$. The numbers for ν and σ_4 are the same as above, $\nu \approx 0.570$ and $\sigma_4 \approx -0.328$.
Plugging everything in expression 2.4, we have

$$\gamma_{\mathscr{G}_2} \approx 1 - 5.130 - 0.656 = -3.956. \tag{3.10}$$

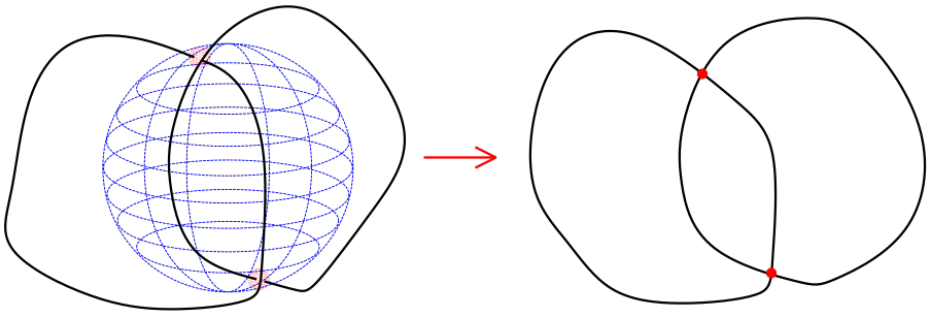

Figure 3.7: If the delocalized linked region of an Hopf link can be described, in the asymptotic limit, by two separated contact points, then we can associate the link to a 4-legged watermelon network. This network is made of two vertices of functionality 4 and 4 branches. The name comes from its shape and is used by Duplantier in his work [2].

Additional configuration factor An additional configuration factor comes from the freedom on the position of the two contact points.
We can try to predict its scaling behavior in powers of N in the large N limit.
We start by fixing the first contact point, operation that contributes with a factor $\sim N^2$, then we have to select a distance (i.e. number of monomers) between the first and second contact ones on both loops. Let us call l_1 and l_2 these distances. Taking into account that the two points of a loop must divide it in two portions both growing as $\mathcal{O}(N)$ in the asymptotic limit, we can say that $\alpha_1 N < l_1 < \beta_1 N$ and $\alpha_2 N < l_1 < \beta_2 N$ for some $\alpha_1, \beta_1, \alpha_2$ and $\beta_2 \in \mathbb{R}$. Hence, selecting l_1 and l_2 brings in another $\sim N^2$ factor. The total additional configuration factor, in the large N limit, goes like $\sim N^4$.
As a result

$$\gamma_{\mathscr{H}} = \gamma_{\mathscr{G}_2} + 4 \approx 0.044. \tag{3.11}$$

Topology As far as topology is concerned, we can argue analogous considerations to those of the previous section. If we want to describe loops with the Hopf topology, we need to fix the unknot topology for the branches of the watermelon networks, as a consequence we need to introduce a new topology dependent exponent $\gamma_{\mathscr{G}_2}(\emptyset)$ and then we can assume, by analogy with knots, that $\gamma_{\mathscr{G}_2}(\emptyset) \approx \gamma_{\mathscr{G}_2}$.

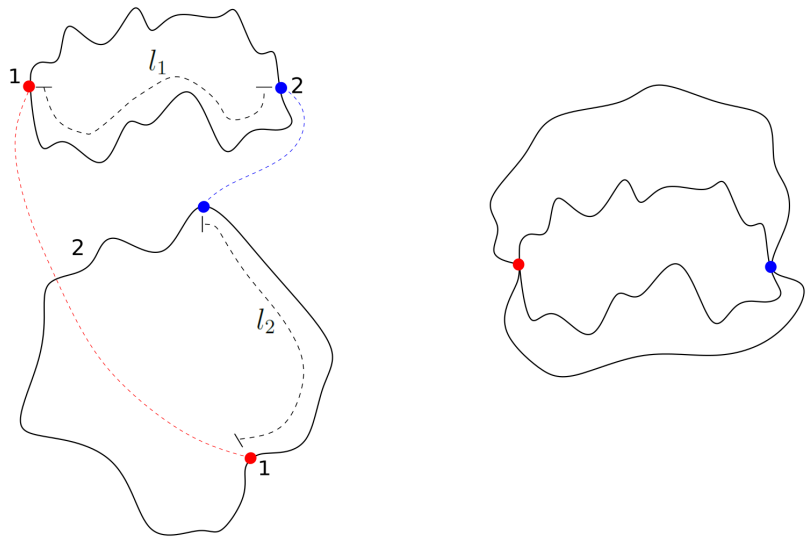

Figure 3.8: The additional configuration factor to adapt the power law for a monodisperse 4-legged watermelon network to a couple of linked loops with the Hopf topology is $\sim N^4$. The selection of the first contact point comes with a factor $\sim N^2$, that of the distances l_1 and l_2, with another $\sim N^2$.

Chapter 4

Simulation Method

In chapter 2, we studied Duplantier's theory on polymer networks and, in chapter 3, we used it to predict the asymptotic behavior of two linked polymer loops in $\mathbb{R}^3$ with the topology of the Hopf link. In order to test what we have done so far, we now want to sample configurations with the Hopf topology and make a comparison between how their number scales with the total length and the predictions of the previous chapter.
In this work, we will make a simulation on the cubic lattice, so we need a method to generate configurations for two linked loops with fixed topology and arbitrary length in $\mathbb{Z}^3$. In this chapter, we are going to illustrate how one can achieve this by choosing an opportune algorithm for generating configurations for a single loop and extending it for our purpose.

4.1 Monte Carlo algorithms

The algorithm we will be using (either for a single loop, the starting one, or the adaptation to a pair) falls under the category of Monte Carlo methods. These aim to sample configurations of self-avoiding walks (loops) by changing them and producing a correlated sequence: they are based on the construction of a Markov chain over the state space made by all the possible walks on a selected lattice, with a limit distribution which is used to sample from it.
From now on, we will be considering only Monte Carlo methods on the cubic lattice.

Markov chains What is a Makov chain, more precisely?
Given a state space $\Omega = \{X_i\}_{i\in\mathbb{N}}$ ($i \in \mathbb{N}$ means that the number of the states X_i is

infinite but numerable[1]), a Markov chain X_t is a discrete time stochastic process on Ω characterized by a compete set of transition probabilities from a generic state $X \in \Omega$ to another $Y \in \Omega$, $p_{XY}(t) = Pr(X_{t+1} = Y | X_t = X)$, which we will assume to be time independent[2] ($p_{XY}(t) \equiv p_{XY}$) with the properties

- $p_{XY} \geq 0 \qquad \forall\, X, Y \in \Omega$
- $\sum_{Y \in \Omega} p_{XY} = 1 \qquad \forall\, X \in \Omega$
- $Pr(X_{t+1} = \bar{X}_{t+1} | X_t = \bar{X}_t) = p_{XY} = Pr(X_{t+1} = \bar{X}_{t+1} | X_t = \bar{X}_t, X_{t-1} = \bar{X}_{t-1}) = Pr(X_{t+1} = \bar{X}_{t+1} | X_t = \bar{X}_t, X_{t-1} = \bar{X}_{t-1}, \dots) \quad \forall \bar{X}_t,\, t = 0, 1, \cdots \in \Omega$

The first two are the usual normalization properties, the third is the memorylessness one: the transition probability to another state depends only on the current state and not on the history of the process.
Starting from a given initial one, $\bar{X}_0$, a system which evolves following a Markov chain goes through a sequence of states with a certain probability distribution, namely, at time $\bar{t}$ fixed, that of $X_{\bar{t}}$, which is an aleatory variable. One of these sequences is a realization of the process.
A probability distribution π_X on Ω is said to be stationary (fixed point) for X_t if it satisfies

$$\sum_{X \in \Omega} \pi_X p_{XY} = \pi_Y \qquad \forall\, Y \in \Omega. \tag{4.1}$$

A fundamental property of a Markov chain is that, for $t \to \infty$, it approaches, regardless of the initial state X_0, under the condition of irreducibility, a unique stationary probability distribution, π_X, on Ω.
Let us be more specific. It can be shown that [16]:

Theorem 4.1. *We define irreducible a Markov chain X_t on Ω satisfying*

$$\forall\, X, Y \in \Omega, \forall\, t \in \mathbb{N}, \exists\, n \in \mathbb{N} \quad t.c. \quad Pr(X_{t+n} = X | X_t = Y) > 0. \tag{4.2}$$

For every given homogeneus and irreducible Markov chain, there is a unique stationary probability distribution.

Theorem 4.2. *Every homogeneus and irreducible Markov chain converges, at fixed t, $t \to \infty$, to its stationary distribution for any given initial distribution probability π_0.*

Note that, in simple words, an irreducible (or ergodic) Markov process on Ω, is one for which every state of Ω can be reached from any other sometime in the future.

[1] For a general Markov chain, this number could also be finite, but here this definition is more appropriate.

[2] The associated Markov chain is said to be homogeneus in this case.

4.2 BFACF algorithm

From what we remembered in the previous section, we understand that what we should search for is an ergodic algorithm, namely one which underlying Markov chain is irreducible, so that we can sample, after a relaxation time, from a unique stationary distribution we should identify.
Madras and Sokal [**?**] proved that no Monte Carlo method which is length conserving and uses only local moves can be ergodic. Hence, we need to work in the grand canonical ensamble, simulating self-avoiding configurations of links of free to vary length.
We are interested in links with a specific topology, so we should aim for a simulation method which ergodicity classes are fixed link types. Note that we are talking of the overall topology, not only how two (or more) loops are linked to each other: the knot type of the components is also included. An algorithm known for having this property, if applied to single self-avoiding polygons (polymer loops on a lattice), is the BFACF (Berg, Foester [17], Aragao de Carvalho, Caracciolo and Fröhlich [18]): Janse van Rensburg and Whittington [19] demonstrated that its ergodicity classes, for loops on the cubic lattice, are knot types.
What we are going to do is to extend the BFACF algorithm for knotted polygons to linked polygons.

4.2.1 BFACF for polygons

The original simulation method acts on the space made by all the possible configurations of any length of self-avoiding, not oriented and unrooted (i.e. without fixed points) polygons on the cubic lattice. It consist in a stochastic sequence of moves that perform local deformations on an initial state. These are the rules:

1. Given a particular polygon configuration $\omega = (\omega(0), \omega(1), \ldots, \omega(N))$, an edge $[\omega(i+1), \omega(i)]$ and an orthogonal direction $\vec{e}$ are chosen at random.

2. If both $x = \omega(i) + \vec{e}$ and $y = \omega(i+1) + \vec{e}$ are not already occupied (self-avoidance), a transformation of type $\Delta(N) = +2$, as in figure 4.1(a), is performed with probability

$$p^{\Delta(N)}(\omega \to \omega') = \min\left(1, \left(\frac{N + \Delta(N)}{N}\right)^{q-1} K^{\Delta(N)}\right). \tag{4.3}$$

   q and K, the step fugacity, are parameters of the algorithm: they are introduced, in the grand canonical ensamble, to regulate the mean value of the length of the configurations sampled, which should be set to be large enough when studying the asymptotic limit. The new configuration will be

(a) (b)

Figure 4.1: The two types of moves performed in the BFACF algorithm for polygons on a cubic lattice. **(a)** Moves of type $\Delta(N) = \pm 2$; they change the total length of a loop by $+\Delta(N)$. **(b)** Flips; they leave the length unchanged.

$\omega' = (\omega(0), \ldots, \omega(i-1), \omega(i), x, y, \omega(i+1), \omega(i+2), \ldots, \omega(N))$, with length $N' = N + \Delta(N) = N + 2$.

3. If both conditions $x = \omega(i-1)$ and $y = \omega(i+2)$ are satisfied, a move of type $\Delta(N) = -2$ is executed, with the same probability. This gives a polygon with $N' = N - 2$.

4. If the conditions $x = \omega(i-1)$ and y is not occupied, or x is not occupied and $y = \omega(i+2)$ are satisfied, than a flip, like in figure 4.1(b), is performed with unitary probability. This transformation is length preserving.

Like we already mentioned, in 3 dimensions the BFACF moves are ergodic on the subspaces made of all and only configurations with fixed knot type τ and, with these probabilities, the asymptotic distribution reached is

$$\pi_\tau(\omega) = \frac{1}{\tilde{G}_q(K,\tau)} N^q K^N \chi(\tau(\omega), \tau), \tag{4.4}$$

where $\tilde{G}_q(K,\tau) = \sum_{N \geq N_{min}} \mathscr{Z}_N(\tau) N^q K^N$ is a normalization factor ($\mathscr{Z}_N(\tau)$ is the number of configurations with length N and topology τ) and χ is the characteristic function.
One can also check its stationarity.

4.2.2 Two linked polygons

BFACF algorithm for two linked polygons Let us now try to extend this algorithm to the case of a pair of linked polygons. The idea is to think of the couple as a single polymer composed by two pieces. We can select, with some probability, one of the two loops or the other and apply the same moves as above, choosing an opportune probability for the $\Delta(N) = \pm 2$ moves. We want only self-avoiding

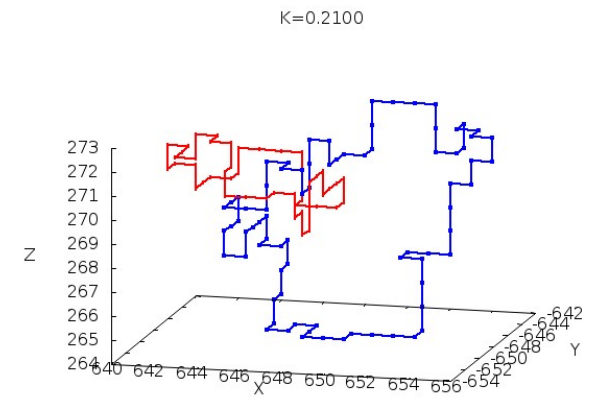

(a)

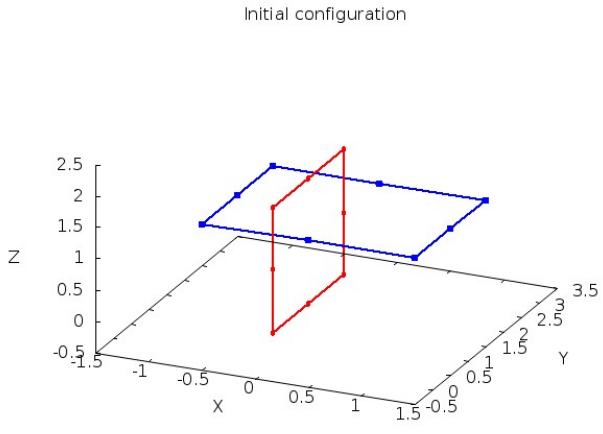

(b)

Figure 4.2: **(a)** An example of a link configuration with the Hopf topology sampled with the extended BFACF algorithm; $K = 0.2100$ and $q = 3$. This was obtained after 10^{10} iterations starting from (b), note how the topology was preserved. **(b)** The starting configuration.

configurations, so we need also to check mutual-avoidance. Hence, we add two new rules and modify the second.

0. Given two linked polygons of lengths N_1 and N_2, one of them is selected with probability $\frac{N_1}{N_1+N_2}$ and $\frac{N_2}{N_1+N_2}$ respectively[3]. We call $\omega = (\omega(0), \omega(1), \ldots, \omega(N))$

[3]They are clearly normalized at 1.

its current configuration.

2(*bis*). If both $x = \omega(i) + \vec{e}$ and $y = \omega(i+1) + \vec{e}$ are not already occupied, a transformation of type $\Delta(N) = +2$ is performed, with probability

$$p^{\Delta(N)}(\omega \to \omega') = \min\left(1, \left(\frac{N_1 + N_2 + \Delta(N)}{N_1 + N_2}\right)^{q-1} K^{\Delta(N)}\right). \tag{4.5}$$

The new configuration will be $\omega' = (\omega(0), \ldots, \omega(i-1), \omega(i), x, y, \omega(i+1), \omega(i+2), \ldots, \omega(N))$, with length $N' = N + \Delta(N) = N + 2$.

5. At every step, a check of mutual-avoidance is needed.

The proof of the ergodicity of this algorithm on the subspace made of all and only the states with a fixed topology is the focus of the next chapter. For now, let us assume that this is true and focus on the research of the stationary distribution. By fixing a topology τ, the limit distribution is

$$\pi_\tau(\omega) = \frac{1}{G_q(K,\tau)}(N_1 + N_2)^q K^{(N_1+N_2)} \chi(\tau(\omega), \tau), \tag{4.6}$$

where $\tilde{G}_q(K,\tau) = \sum_{N_1,N_2} \mathscr{Z}_{N_1,N_2}(\tau)(N_1+N_2)^q K^{(N_1+N_2)}$.

Stationarity Let us check that this probability distribution is indeed stationary. We will achieve this by showing that $\pi_\tau(\omega)$ satisfies detailed balance:

$$\pi_\tau(\omega) p_{\omega\omega'} = \pi_\tau(\omega') p_{\omega'\omega} \qquad \forall\, \omega, \omega' \in \Omega. \tag{4.7}$$

Note that this is a stronger condition than the stationarity one 4.1. Ω is the state space and $p_{\omega\omega'}$ the transition probability[4] from state ω to state ω'

$$p_{\omega\omega'} = \begin{cases} p_\sigma & \exists\, \sigma \in S \quad t.c. \quad \omega' = \sigma\, \omega \\ 0 & otherwise \end{cases}, \tag{4.8}$$

where S is the ensemble of all possible BFACF moves on ω.

Type ± 2 moves We start from a move of type $+2$ on the first polygon of the couple, that of length N_1, which is selected with probability $\frac{N_1}{N_1+N_2}$.
First a random side of the configuration ω is identified (with probability $\frac{1}{N_1}$), if a move of this type cannot be applied, $p_{+2} = 0$ and 4.7 is trivially true; otherwise,

[4]These are defined for only one iteration, so if ω' can not be obtained from ω with one single BFACF move, $p_{\omega\omega'} = 0$.

a transformation with acceptance probability $a_{+2}(\omega \to \omega')$ is attempted.
We can find $a_{+2}(\omega \to \omega')$ by imposing the detailed balance 4.7, so we can check if we get 4.5.

$$\frac{N_1}{N_1+N_2}\frac{1}{N_1}a_{+2}(\omega \to \omega')\pi_\tau(\omega) = \frac{N_1+2}{N_1+N_2+2}\frac{1}{N_1+2}a_{-2}(\omega' \to \omega)\pi_\tau(\omega') \quad (4.9)$$

By plugging in expression 4.6 of $\pi_\tau(\omega)$, we get

$$\begin{aligned}&\frac{1}{N_1+N_2}\frac{1}{G_q(K,\tau)}(N_1+N_2)^q K^{(N_1+N_2)}a_{+2}(\omega \to \omega') \\ &\quad = \frac{1}{N_1+N_2+2}\frac{1}{G_q(K,\tau)}(N_1+N_2+2)^q K^{(N_1+N_2+2)}a_{-2}(\omega' \to \omega),\end{aligned} \quad (4.10)$$

so

$$\frac{a_{+2}(\omega \to \omega')}{a_{-2}(\omega' \to \omega)} = \left(\frac{N_1+N_2+2}{N_1+N_2}\right)^{q-1} K^2. \quad (4.11)$$

This relation does not completely fix the probability a_{+2}. One common solution is the Metropolis choice [20]; in this case it reads

$$a_{+2}(\omega \to \omega') = \min\left(1, \left(\frac{N_1+N_2+2}{N_1+N_2}\right)^{q-1} K^2\right) \quad (4.12)$$

This is valid for every configurations ω and any $+2$ move on it; it depends only on the length of the polymers of ω.
Finally, by repeating the same procedure for a -2 move, one would obtain the expected result

$$a_{\Delta(N)}(\omega \to \omega') = \min\left(1, \left(\frac{N_1+N_2+\Delta(N)}{N_1+N_2}\right)^{q-1} K^{\Delta(N)}\right), \quad (4.5)$$

$\Delta(N) = \pm 2$. Note that this is consistent with what we would get for a_{-2} from 4.11 and 4.12.
The same result is achieved for ± 2 moves on the second polymer.

Flips Given that the probability density function 4.6 depends only on the lengths of the two linked polygon and that a flip move does not change these lengths, the same calculations as above would give an unitary acceptance probability for flips.

4.3 Multiple Markov chains

The above results imply that the Markov chain underlying the algorithm eventually (i.e. in the long time limit) converges to the stationary distribution. However, the convergence can be extremely slow. To improve the mobility of the Markov chain, one can introduce specific sampling techniques.
Propositions 4.1 and 4.2 hold true only for Markov processes, even though we are talking about algorithms that maintain a certain autocorrelation time and are not memoryless. The BFACF algorithm for polygons, for example, is characterized by infinite equilibrium approach time and long correlation times [21].
A way to reduce the autocorrelation times in order to improve the mobility of the BFACF algorithm is based on the so called multiple Markov chains method. It consists in considering several Markov chains running in parallel with different fugacities and trying to swap the states of neighbor chains after a given time.
The ergodicity of this multiple system, as well as detailed balance for the BFACF moves, is granted by that of the single chains (as long as the topology is the same for all the objects considered); so, all we have to do is set a swapping probability that preserves the stationarity of the distribution 4.6. Let's establish a new rule

6. We consider l couples of linked polygons with the same fixed topology and apply BFACF moves to each one of them with different but similar fugacities $\{K_i\}_{i=1,\dots,l}$. Every t_{swap} iteration, we swap the states ω_i and ω_{i+1} of neighbor links with probability

$$p_{swap}(\omega_i \to \omega_{i+1}; K_i, K_{i+1}) = \min\left(1, \left(\frac{K_i}{K_{i+1}}\right)^{N_1^{i+1}+N_2^{i+1}-N_1^i-N_2^i}\right), \quad (4.13)$$

where N_1^{i+1}, N_2^{i+1}, N_1^i and N_2^i are the lengths of the two $(i+1)^{th}$ and i^{th} polygons.

Stationarity Let us check that the probability 4.13 satisfies detailed balance. If we consider a state ω for the i^{th} chain, the swapping to state ω_{i+1} can be done only if the $(i+1)^{th}$ link is in said state. If we call $a_{swap}(\omega_i \to \omega_{i+1}; K_i, K_{i+1})$ the acceptance probability of the swapping, than

$$p_{swap}(\omega_i \to \omega_{i+1}; K_i, K_{i+1}) = \pi_\tau^{i+1}(\omega_{i+1}) a_{swap}(\omega_i \to \omega_{i+1}; K_i, K_{i+1}).$$

Hence, the detailed balance reads

$$\begin{aligned} &\pi_\tau^i(\omega_i)\pi_\tau^{i+1}(\omega_{i+1}) a_{swap}(\omega_i \to \omega_{i+1}; K_i, K_{i+1}) \\ &\quad = \pi_\tau^i(\omega_{i+1})\pi_\tau^{i+1}(\omega_i) a_{swap}(\omega_{i+1} \to \omega_i; K_i, K_{i+1}). \end{aligned} \quad (4.14)$$

Inserting expression 4.6 of $\pi(\omega)$ in this relation, we get

$$(N_1^i + N_2^i)^q K_i^{N_1^i+N_2^i} (N_1^{i+1} + N_2^{i+1})^q K_{i+1}^{N_1^{i+1}+N_2^{i+1}} \frac{a_{swap}(\omega_i \to \omega_{i+1}; K_i, K_{i+1})}{G_q(K_i,\tau)G_q(K_{i+1},\tau)}$$
$$= (N_1^{i+1} + N_2^{i+1})^q K_i^{N_1^{i+1}+N_2^{i+1}} (N_1^i + N_2^i)^q K_{i+1}^{N_1^i+N_2^i} \frac{a_{swap}(\omega_{i+1} \to \omega_i; K_i, K_{i+1})}{G_q(K_i,\tau)G_q(K_{i+1},\tau)}, \tag{4.15}$$

that simplifies in

$$\frac{a_{swap}(\omega_i \to \omega_{i+1}; K_i, K_{i+1})}{a_{swap}(\omega_{i+1} \to \omega_i; K_i, K_{i+1})} = \left(\frac{K_i}{K_{i+1}}\right)^{N_1^{i+1}+N_2^{i+1}-N_1^i-N_2^i}. \tag{4.16}$$

At last, making the Metropolis choice, we get the announced result

$$a_{swap}(\omega_i \to \omega_{i+1}; K_i, K_{i+1}) = \min\left(1, \left(\frac{K_i}{K_{i+1}}\right)^{N_1^{i+1}+N_2^{i+1}-N_1^i-N_2^i}\right). \tag{4.13}$$

4.4 BFACF for several linked polygons

As a final remark, note that the BFACF algorithm applied two linked polygons can be easily extended to an arbitrary number r of self-avoiding links made of polymer loops of lengths N_i, $i = 1, \ldots, r$. The irreducibility for fixed topology still holds, as we will see in the next chapter, while, by applying the same arguments as above, we can obtain a stationary distribution and acceptance probabilities by those valid in the $r = 2$ case with the substitution

$$N_1 + N_2 \to N_1 + N_2 + \cdots + N_r. \tag{4.17}$$

Chapter 5

Ergodicity Properties of the BFACF Algorithm for Linked Polygons

In the previous chapter we have seen how to adapt the BFACF algorithm to sample configurations of a generic number of linked polygons.
We proved the stationarity of a suitable probability distribution and we stated it was the unique asymptotic limit of the underlying Markov chain, implying its irreducibility. The purpose of this chapter is to prove this property.
It has been shown by Madras that the BFACF algorithm is ergodic for polygons on the squared lattice in 2 dimension [22], while Janse van Rensburg and Whittington proved that the ergodicity classes of said algorithm on the cubic lattice (3 dimensions) are polygons with fixed knot type [19].
Here, by following the procedure adopted in [19], we extend the above result, proving the following statement:

Proposition 5.1. *The ergodicity classes of the BFACF algorithm for linked polygons on the cubic lattice in 3 dimensions are made of all and only the configurations with fixed link type.*

5.1 Definitions: links and linked polygons

Let us start with some definitions.

Definition 5.1. *Knot* We define a knot as an embedding $f : S^1 \to \mathbb{R}^3$ (a bijective homeomorphism) of the circle S^1 in the Euclidian 3 dimensional space; we write this map as $(f; S^1, \mathbb{R}^3)$. If we give an orientation the circle S^1 we get an oriented knot.

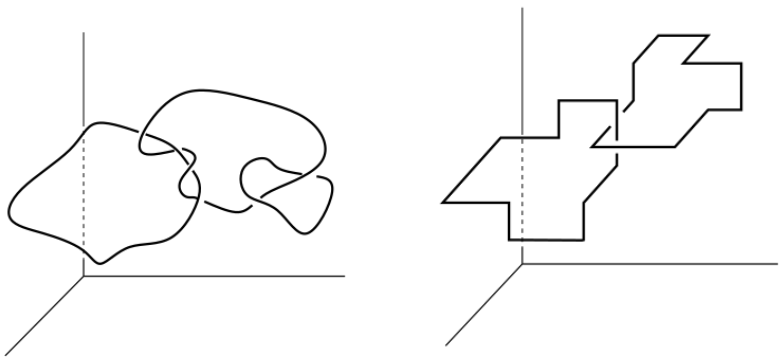

(a) (b)

Figure 5.1: **(a)** A collection of two or more knots, embeddings of the circle S^1 in $\mathbb{R}^3$, whose images do not intersect is a link. This one is made by three linked unknotted loops **(b)** If the embeddings are piecewise linear, we have a set of linked polygons. In this figure, we can see two linked polygons with the topology of the Hopf link.

Definition 5.2. *Polygon* A polygon is a piecewise linear embedding of S^1 in $\mathbb{R}^3$.

Definition 5.3. *Link and linked polygons* We are interested in linked polygons. A link is a collection of knots whose images in $\mathbb{R}^3$ do not intersect, they can either be linked together or not. Hence, linked polygons are a collection of mutual avoiding polygons[1].

Two set of linked polygons (links) are said to be equivalent if they are ambient isotopic, this figuratively means if we can continuously (without breaking or cutting them) deform their image in $\mathbb{R}^3$ one into the other. Through this relation we can group linked polygons (links) into equivalence classes that we call link types.

Definition 5.4. *Link type* Link types are the classes of equivalence of ambient isotopic links.

Definition 5.5. *Regular projection* We call regular the projection of a link on any plane $\mathbb{R}^2 \subset \mathbb{R}^3$ that contains only a finite number of multiple points (points corresponding to more than one of the link), all multiple points have multiplicity 2 (double points) and no vertex is mapped onto one of these (see figure 5.2).

[1]Note that we could assign an orientation also to links, but we will not do that.

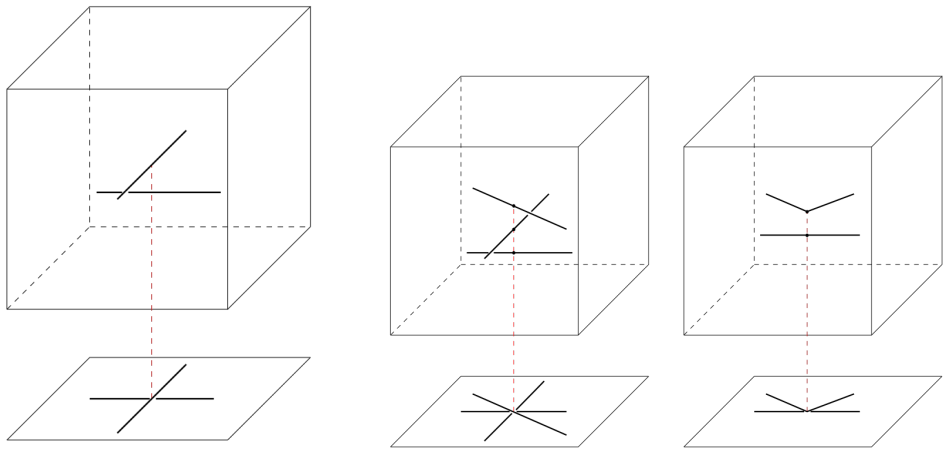

(a) (b)

Figure 5.2: **(a)** This is how a crossing in the regular projection of a link should look like: the edges are X-shaped, with the crossing point corresponding to only two points of the link, none of which a vertex. **(b)** In the other two figures we can see example of possible projected points which violate the regular condition. On the left, more than 2 points of the link are mapped to the same one, on the right a vertex is mapped into a double point.

If we specify at each crossing point of a projection which is the overpassing and the underpassing line (they can either be part of the same knot or not), than we can reconstruct the link (its type) from its regular projection.

Definition 5.6. *Link diagram* A regular projection with underpasses and overpasses specified is called link diagram.

We shall define equivalence classes for link diagrams.

Definition 5.7. *Equivalent link diagrams* We define two link diagrams to be equivalent if they are connected by a sequence of transformation consisting in planar ambient isotopies (i.e. ambient isotopies on the plane $\mathbb{R}^2$ of the projection) and the three type $\Omega 1$, $\Omega 2$ and $\Omega 3$ of local moves called Reidemeister moves, illustrated in figure 5.3.

Reidemeister moves and planar ambient isotopies on a projection of a link are obtained through ambient isotopies on the link itself, so equivalent diagrams are associated to equivalent links. The converse is also true (for links, not only for knots), as proved by Reidemeister [23]. In this way, a correspondence is established between equivalence classes of links and those of link diagrams.

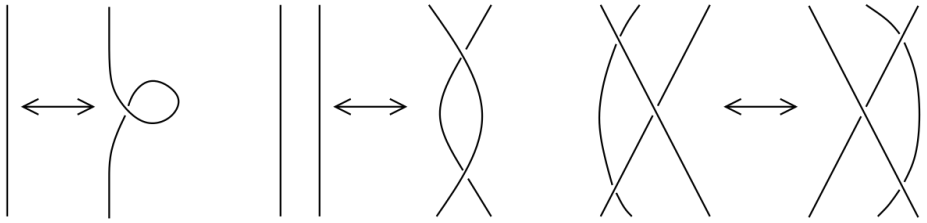

Figure 5.3: The three Reidemeister moves: from left to right Ω1, Ω2 and Ω3. Two equivalent links diagrams are connected by a sequence of these moves and planar ambient isotopies.

Theorem 5.1. *Two links provided with link diagrams are equivalent if and only if their diagrams are equivalent.*

We are not interested in links in general: we will consider only equivalence classes for linked polygons in the cubic lattice ($\mathbb{Z}^3$), so we need to modify the definition of link diagram.
We need the following notation

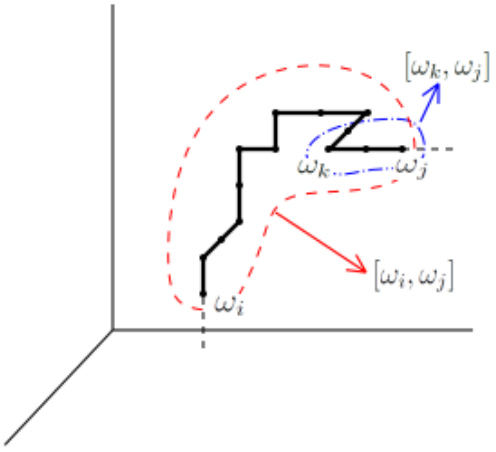

Figure 5.4: $[\omega_i, \omega_j]$, the set of edges of a polygon delimited by vertices $\omega_i, \ldots, \omega_j$, is a segment. $[\omega_k, \omega_j]$, a line segment, is called side.

Definition 5.8. *Segment and side* A segment $[\omega_i, \omega_j]$ of a polygon (linked or not) is the set of edges delimited by the vertices $\omega_i, \omega_{i+1}, \ldots, \omega_j$ if $i \leq j$ or the union

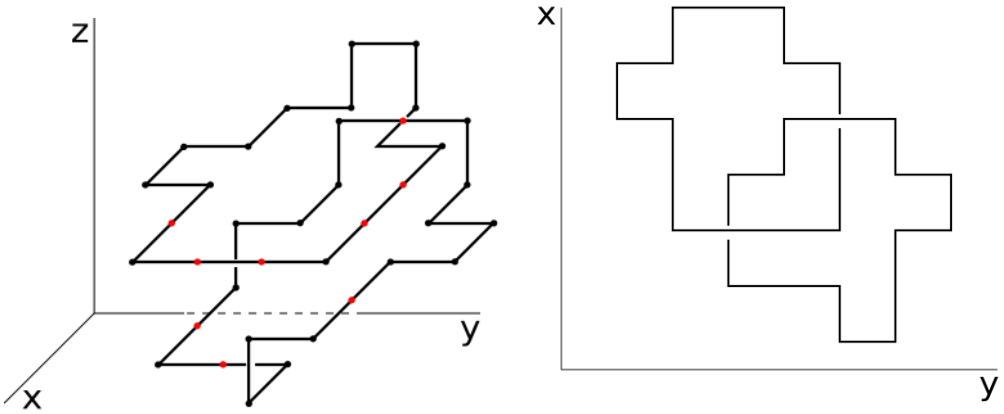

(a) (b)

Figure 5.5: **(a)** Two linked polygons in $\mathbb{Z}^3$ and **(b)** their lattice link diagrams. Note that from the diagrams one can reconstruct the link up to the edges parallel to the z axis. When building the diagram of a set of polygons in the cubic lattice, we consider as vertices only these at the edge of maximal sides (the black ones as opposed to the red ones), otherwise, at crossings, some would be projected to double points.

of $[\omega_i, \omega_N]$ and $[\omega_0, \omega_j]$ if $j < i$ (N is the total number of the monomers of the polygon).
A side is a line segment (see figure 5.4).

Let $\{\vec{e_1}, \vec{e_2}, \vec{e_3}\}$ be an orthonormal basis of $\mathbb{R}^3$. We consider linked polygons with vertices on integer coordinates (x, y, z) with respect to some fixed origin. A projection on the plane $z = 0$ will not be regular in the sense of the definition given above, unless we forget about edges parallel to the z axis and we call vertices only those at the border of maximal sides building the polygons in consideration.

Definition 5.9. *Lattice link diagram* We call lattice link diagram into the plane $z = 0$ the projection, obtained without considering edges parallel to the z axis and vertices inside a maximal side of a set of linked polymers on the cubic lattice, if it is regular.

We assume that theorem 5.1 holds true for lattice link diagrams[2].

[2]We can always do an infinitesimal transformation of the edges parallel to the z axis in order to obtain equivalent links in $\mathbb{R}^3$ with regular projection.

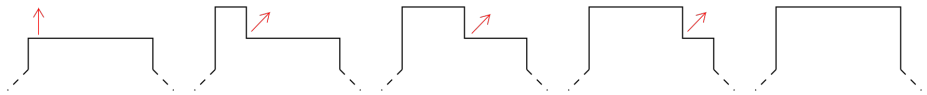

Figure 5.6: Through BFACF operations, it is possible to shift a side of one unit along a perpendicular direction. In this example, a +2 move followed by a sequence of 3 flips is executed (from left to right) in order to achieve this.

5.2 Ergodicity classes

Let us first note that BFACF moves in $\mathbb{R}^3$ are ambient isotopies, because they are continuous deformations; hence

Proposition 5.2. *Ergodicity classes for the BFACF algorithm for linked polygons in 3 dimensions on the cubic lattice are made of configurations of the same link type.*

We need to prove that every configuration of the same link type is contained in the same ergodic class. To do so we will show that two generic set of linked polygons of the same link type can be mapped one into the other by BFACF moves.

1. We will show first that two arbitrary configurations of linked polygons with the same lattice link diagram can be mapped, by BFACF moves, one into the other;

2. that all linked polygons sets can be modified, by BFACF operations, into one with lattice link diagram,

3. and that we can, given two sets of the same link type and with lattice link diagram, change, through BFACF moves on the links, their projection into the same lattice link diagram.

The constructions we are going to do are similar to the ones given in [19], but applied to a set of linked polygons as a whole.

First step In order to show the first point, we note that

Proposition 5.3. *Given a side of a polygon and enough space, it is possible, through BFACF operations, to shift it one unit along a perpendicular direction in the cubic lattice.*

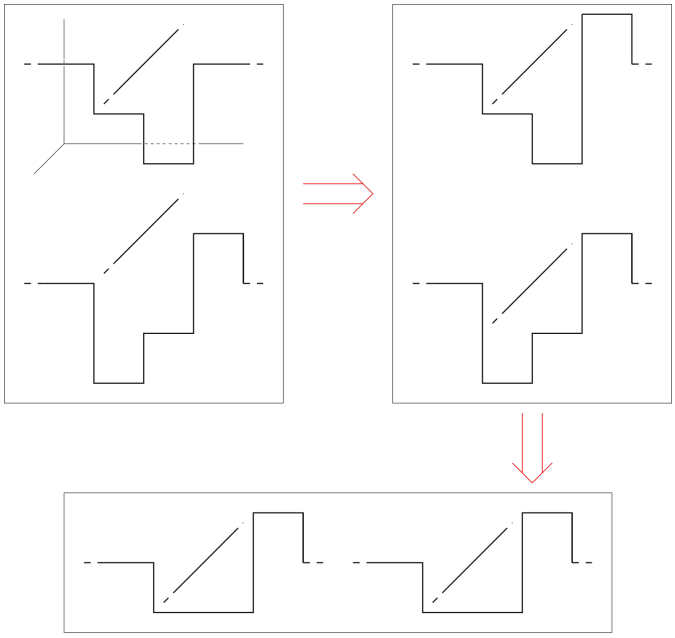

Figure 5.7: We can make identical, by BFACF moves, two sets of linked polygon with the same lattice link diagram. In order to do so, we first have to rise all edges of both sets, with the exception of these involved in underpasses, to a common position, like shown in the upper right box of the figure, then we have to raise all underpasses a unit under the corresponding overpassing edges, like shown in the bottom box.

An example of how this shift is performed is shown in figure 5.6.
With this, we can prove the following result:

Proposition 5.4. *Let ω and ν be two sets of linked polygons in $\mathbb{Z}^3$ with identical lattice link diagram. There exist a sequence of BFACF moves which connects ω to ν.*

Proof. A lattice link diagram is a collection of linear segments on a plane, each one corresponding to a number of sides of the projected polygons (edges perpendicular to the projection plane are mapped to a point), with overpasses (ad underpasses) specified. By definition, in a lattice link diagram (it is a regular projection), there are not double edges and each crossing, being it made by two sides of the same polygon or not, is cross-shaped.
Let us consider a line segment in the common projection. Let us assume it contains l underpasses at positions $\{k_i\}_{i=1,\dots,l}$. Using proposition 5.3, we can rise all the edges of the corresponding sides of ω and ν, with the exception of the segments corresponding to the underpasses (in the projection they are $\{k_i - 1, k_i + 1\}, i =$

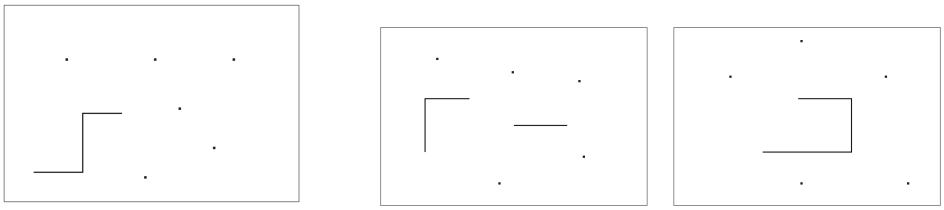

(a) (b)

Figure 5.8: This is what a plane perpendicular to the projection plane of a set of linked polygon in standard form should contain of that set. **(a)** This is the correct situation: only one segment and a finite number of disjoint points. **(b)** The other two figures are taken from a set not in the standard form. On the left we have more than one segment, on the right a segment whose projection contains double edges.

$1, \ldots, l$) to a common established position in the lattice (note that there is always space for this, by construction). We repeat this procedure for all the segments of the projection. Now the two sets of polygons only differ at underpasses. If now we raise the sides containing the underpasses a unit under the overpasses in both ω and ν, we are done. This procedure is illustrated in figure 5.7

Second step We shall now show how one can always change, by BFACF moves, a set of linked polygons to give it a lattice link diagram. If we prove this, than we can consider only sets with lattice link diagram and forget about the others.
The way to go is showing that we can always put a set of linked polygons in standard form, which has, by construction, lattice link diagram.

Definition 5.10. *Standard form* Consider a set of linked polygons ω. If every plane T which intersect the projection plane $z = 0$ at 90° contains at most a finite number of disjoint points (sides that pass through it) and at most one segment of ω, and if the projection of ω contains no multiple edges, then we say that ω is in standard form (figure 5.8).

To show this we need to be able to make as much space as we want

Proposition 5.5. *Let $T_i(a)$, $i = 1, 2$ be the plane perpendicular to $\vec{e_i}$ with coordinate $x_i = a$. Let ω be a set of linked polygons. The plane $T_i(m + \frac{1}{2})$, $m \in \mathbb{Z}$ intersect ω in a finite number of points belonging to its sides. We can use BFACF moves to add an edge to each of the sides intersected by this plane (figure 5.9).*

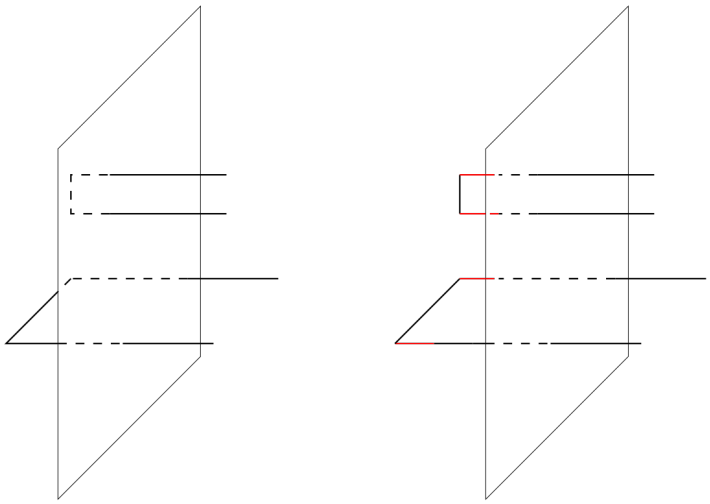

Figure 5.9: Given a set of linked polymers ω and a plane perpendicular to one of the directions orthogonal to the projection axis, it is always possible, by BFACF moves, to add an edge to each side of ω passing through it.

Proof. Consider the vertex with the maximum coordinate $x_i = x_{max}$ among all the vertices on all polygons of the set and the plane T_i through it. Using proposition 5.3, we can move all the segments of the set (it does not matter which polygon they belong to) contained into this plane by one unit in the direction $\vec{e}_i$ (there is enough space, because we are considering the maximum coordinate). By doing this, we are opening space to do the same for the coordinate $x_{max} - 1$ and so on, until $m + 1$ included. We have, in this way, added an edge to all the sides passing through $T_i(m + \frac{1}{2})$.

A direct application of propositions 5.3 and 5.5 is

Proposition 5.6. *Let ω be any set of linked polygons. We can apply BFACF moves to transform it into one in standard form.*

Proof. Any plane perpendicular to the projection axis, but not to either $\vec{e}_1$ or $\vec{e}_2$ will not contain segments of ω, but only finitely many points. So we have only to consider the intersection between ω and planes perpendicular to one of $\vec{e}_1$ or $\vec{e}_2$. Let us consider first $\vec{e}_1$. A generic plane will contain a finite number of points and segments (of any of the polygon of the linked set). If the plane passing through coordinate m, $m \in \mathbb{Z}$, $T_1(m)$, contains l segments, by proposition 5.5, we can move away every segment at coordinates $m + 1, m + 2, \ldots, m + l - 1$ and, by proposition 5.3, we can shift each segment in $T_i(m)$, to a different plane

among $T_1(m), \ldots, T_1(m+l-1)$. Repeating this for every plane, we get a set with no more than one segment in every plane perpendicular to $\vec{e}_1$. If one of these segments contains pieces projected to double edges, we can, again, make room with proposition 5.5 and split it to different planes until there are no more double edges in its projection.
If we repeat the same construction for the planes perpendicular to $\vec{e}_2$, we get a set of linked polygons in standard form. Note that we are considering finite polygons, so at some point this process must end.

We can then state the following:

Corollary 5.6.1. *Using BFACF moves, we can transform any set of linked polygons ω into one with lattice link diagram.*

Third step The last thing to do is to connect lattice link diagrams of sets of the same link type. Let us start from showing that we can execute the three type of Reidemeister moves by BFACF transformations.

$\Omega 1$ We are dealing with a segment which starts in an overpass (underpass) and ends in an underpass (overpass) at the same location in the lattice, without any other crossing. Let us call $[\omega_i, \omega_j]$ this segment and set $i < j$ without loss of generality. After making enough room by using proposition 5.5, we can lift every edge in the segment $[\omega_i, \omega_{j-2}]$ to the same ordinate. Since the BFACF algorithm is ergodic in 2 dimensions [22], we can operate on the segment $[\omega_i, \omega_{j-2}]$, which is a planar one, until it consists only of the edge $[\omega_i, \omega_{j-2}]$. A -2 move completes the construction. The opposite move is done by inverting this construction after making enough space. This procedure is illustrated in figure 5.10.

$\Omega 2$ We have two segments which start at a crossing and end at a crossing. At both crossing, the first (second) of the two segment passes over the other. To perform the move we need first to create a suitable area, Q, free of projected edges using, as always, proposition 5.5. We can then make the first (second) segments planar, by construction 5.3 and use the ergodicity on the plane to move this segment in the free area. The inverse move is performed in the same way. See figure 5.11 for reference.

$\Omega 3$ The procedure to perform this move and its opposite is analogous to that used for $\Omega 2$. We just need to clear an opportune area. This is illustrated in figure 5.12.

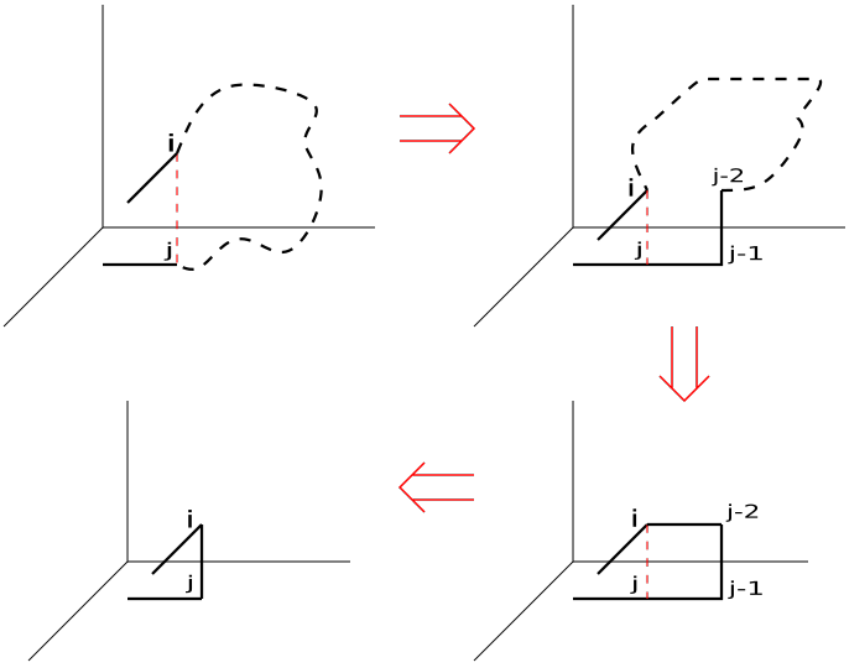

Figure 5.10: This is how we can execute the move Ω1 by a sequence of BFCF operations. The order is clockwise. We lift a portion of the segment to a plane as in the second figure and use the ergodicity of the BFACF algorithm in 2 dimensions.

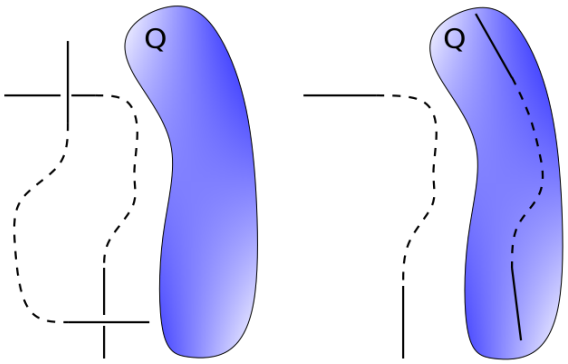

Figure 5.11: The move Ω2 performed with BFACF operations. After creating a free area Q, it is sufficient to make the upper segment planar and use the ergodicity of the BFACF algorithm in the plane.

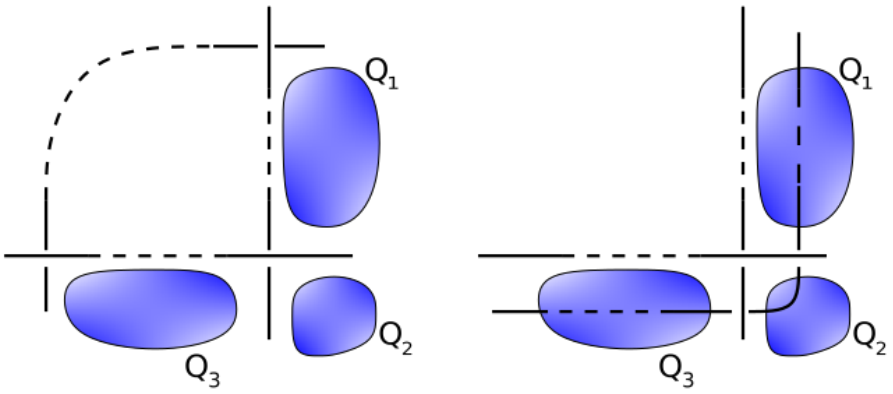

Figure 5.12: The move Ω3 executed with BFACF operations. This time we need to create the three free areas Q_1, Q_2 and Q_3 and then move the lowest segment as done for the move Ω2.

Proposition 5.7. *Let ω and ν be two set of linked polygons of the same link type with lattice link diagrams W and V respectively. By applying BFACF moves, we can transform ω in a set ω' with lattice link diagram W' such that there exist a plane isotopy connecting W' and V.*

Proof. If ν and ω are of the same link type, then we know that V and W are equivalent (as we noted before, edges parallel to the projection axis are only a formal problem). Consequently, we can transform ω using Reidemeister moves so that its new projection differs from V only by a plane isotopy; we can perform these moves with BFACF operations as noted above. If we then apply corollary 5.6.1, we get the set ω' we were searching for.

The last thing to check is that we can make two isotopic lattice link diagrams by using BFACF moves on the correspondent sets of linked polygons. This involves two phases. The first is a comparison of the two projection edge by edge, the second is a translation of one of the two sets.
Proving that, by BFACF moves, we can translate in a certain oriented direction $\pm\vec{e}_i$, $i = 1, 2, 3$ a set of linked polygons is simple: we need to apply proposition 5.5 in a sequence starting from the maximum or minimum (it depends on the sign of the translation) coordinate x_i among those of every vertex of the set, and repeat this as many times as needed.
The comparison edge to edge is a bit long. It consists in identifying corresponding areas in the two lattice link diagrams (since they are isotopic, we can always do that) and modify one of the two sets so that the areas in its projection, one by

one, become of the same shape as the equivalent ones in the other projection. A detailed description of this procedure applied to knots can be found in [19]. When considering sets of linked polygons instead, the difference is that there will be areas with perimeter made by the projections of edges belonging to different polygons. This, however, does not prevent to identify correspondent areas in the isotopic diagrams.
To sum it up,

Proposition 5.8. *Let ω and ν be two sets of linked polygons of the same link type with lattice link diagram. We can always apply BFACF moves to one of them in order to transform its diagram into the other.*

Conclusion By combining proposition 5.4, 5.8 and corollary 5.6.1, we have the proof of the following statement:

Proposition 5.1. *The ergodicity classes of the BFACF algorithm for linked polygons on the cubic lattice in 3 dimensions are made of all and only the configurations with fixed link type.*

Chapter 6

Simulation and Numerical Results

By using the extension of the BFACF algorithm illustrated in chapters 4 and 5, we can simulate configurations of linked polygon pairs with fixed topology in the grand canonical ensamble (i.e. total length-varying).
According to the prediction we made in chapter 2, the number of configurations of a pair of linked loops with total length N and with the Hopf topology, $\mathscr{H}$, scales, in the asymptotic limit, as

$$\mathscr{Z}_N(\mathscr{H}) \sim \mu^N N^{\gamma_{\mathscr{H}}-1} \qquad (N \gg 1), \tag{3.1}$$

where

- $\gamma_{\mathscr{H}} = -0.748$ in the monodisperse case (both loops forming the link have $\mathcal{O}(N)$ length) if the linked portion, in the asymptotic limit, is localized (figure 6.1(a));
- $\gamma_{\mathscr{H}} = -0.763$ in the polydisperse case (one loop has $o(N)$ length; figure 6.1(b));
- $\gamma_{\mathscr{H}} = 0.044$ in the monodisperse case if the linked portion is delocalized with two contact points (figure 6.1(c)).

In chapter 4, we stated that the sampling probability distribution of the BFACF algorithm, fixing the Hopf topology (i.e. starting from an initial configuration with this topology), is, for a configuration ω with topology $\tau(\omega)$,

$$\pi_{\mathscr{H}}(\omega) = \frac{1}{G_q(K,\tau)} N^q K^N \chi(\tau(\omega), \mathscr{H}), \tag{4.6}$$

where $\tilde{G}_q(K,\tau) = \sum_N \mathscr{Z}_N(\mathscr{H}) N^q K^N$ is the normalization factor and χ the characteristic function.

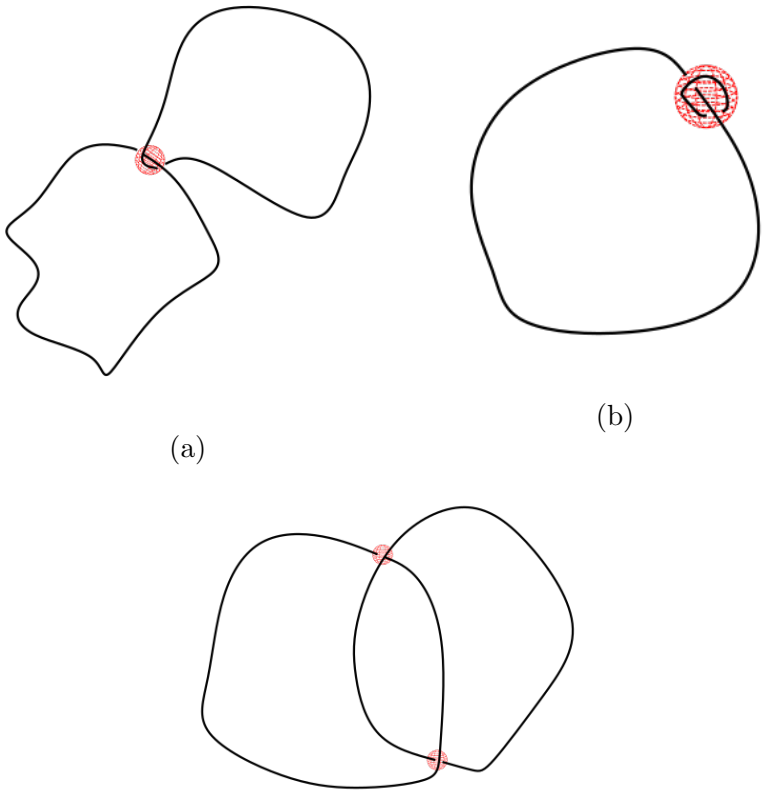

(a) (b) (c)

Figure 6.1: **(a)** A reminder of how a monodisperse link with the Hopf topology and localized linked portion looks like. **(b)** A ploydisperse Hopf link. **(c)** Example of a monodisperse Hopf link with delocalized linked region with two contact points.

We expect the number of sampled polygon pairs, $\mathscr{Z}_N^s(\mathscr{H})$, with total length N and the Hopf topology to scale, in the large N limit, as

$$\mathscr{Z}_N^s(\mathscr{H}) \sim N^{\gamma_{\mathscr{H}}+q-1}(\mu K)^N. \tag{6.1}$$

To test our predictions, we need to check if, indeed, $\mathscr{Z}_N^s(\mathscr{H})$ is properly fitted by this expression: if the answer is affirmative, then we have shown that we can use Duplantier's results on polymer networks to describe the asymptotic behavior of Hopf links.
From the data we will gather, we will calculate μ; if it is the same of the one appearing in the scaling law of networks, its value should be compatible with the Guttmann estimate, $\mu = 4.68393 \pm 0.00002$, we mentioned in chapter 1. Our final goal, however, is to compare $\gamma_{\mathscr{H}}$ with the predicted values obtained analytically in

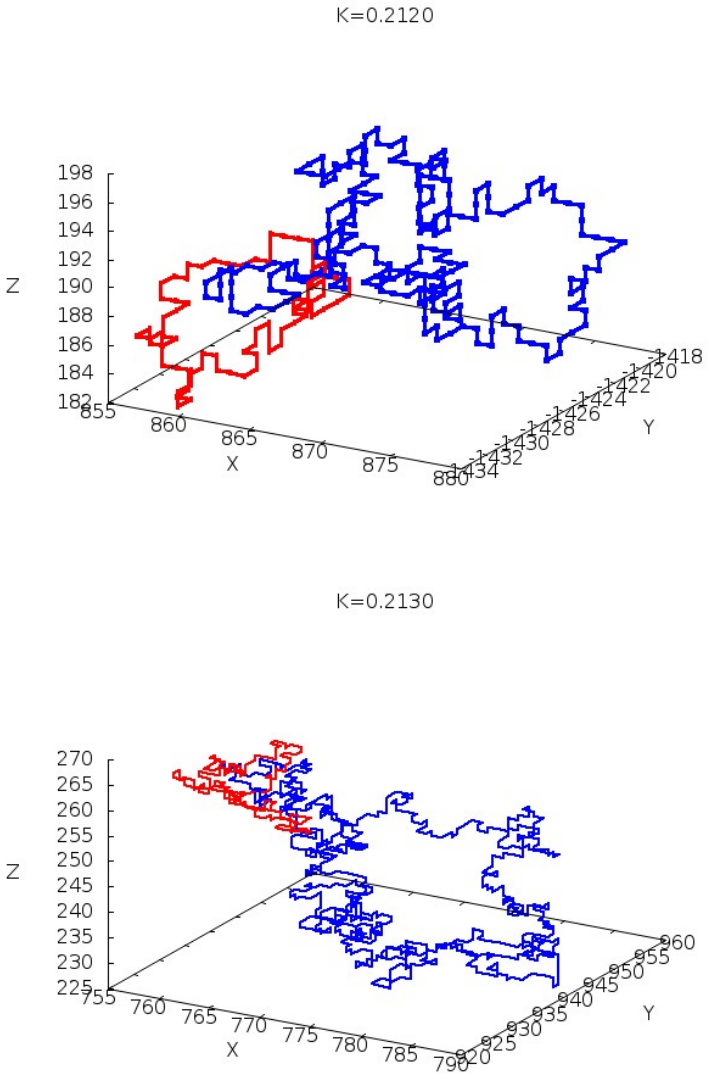

Figure 6.2: An example of two configurations sampled respectively at $K = 0.2120$ and $K = 0.2130$. Note that one of the two loops of the second configuration is significantly smaller than the other, suggesting polydispertion.

chapter 3 and then argue if the linked portion of an Hopf link, in the asymptotic limit, is localized or not.

6.1 Simulation parameters

We sampled, after a relaxation time of 10^9 BFACF iterations, $5 \cdot 10^4$ configurations, one every 10^6 attempted moves, for 8 chains using the multiple Markov chains method; the swapping of configurations between neighbor chains was attempted every 10^3 iterations. The total number of attempted BFACF moves was $4.08 \cdot 10^{11}$.
To choose the values of the step fugacity for each chain, we argued as follows. In appendix B, we showed that the expected mean total length of configurations sampled with a given K is

$$\begin{aligned} \langle N \rangle_q(K, \mathscr{H}) &\approx a(\mathscr{H}) \mu K (1 - \mu K)^{-1} \\ a(\mathscr{H}) &= \gamma_{\mathscr{H}} + q. \end{aligned} \tag{6.2}$$

Since we are interested in sampling configurations with sufficiently large N, we need to set a value of K so that $\langle N \rangle_q(K, \mathscr{H})$ is large enough. From equation 6.2, we see that the mean length diverges for a critical value of the step fugacity: $K_c = \mu^{-1}$. This value depends on μ, which is not known a priori for a link topology. To start off, we can assume that μ for the Hopf topology is very close to the Guttmann estimate, $K_c = 0.213496 \pm 0.000009$, and select values of $K \lesssim K_c$. From the sampling we can then extract an estimate of the real value of μ and retune the simulation parameters K accordingly. We will see that, within statistical errors, our estimate of μ for the Hopf link topology coincides with the Guttmann one, so recalibrating the step fugacities was not necessary.
Another thing to consider in selecting K is that even though the closer it is to K_c the larger the mean length is, the larger the correlations between the sampled configurations, hence the fluctuations, get. When N is large, more BFACF moves are needed to modify a configuration in a significantly different one: if the number of iterations between two sampled configurations is not large enough, this could give rise to strong correlations between subsequent samplings.
Qualitatively, this can be seen in the plot of $\mathscr{Z}_N^s(\mathscr{H})$ over N for different step fugacities and numbers of BFACF iterations between samplings. These are shown respectively in figures 6.3 and 6.4. A more quantitative way to look at this is through the autocorrelation time, that can be estimated as follows.
Given a sample of n chronologically ordered observations, $\{X_s\}_{s=1,\dots,n}$, of a generic observable O, we define its autocorrelation function as[1]

$$f_O(t) = \frac{\langle \, (O(X_s) - \langle O(X_s) \rangle)(O(X_{s+t}) - \langle O(X_s) \rangle) \, \rangle}{\sigma^2_{O(X_s)}}.$$

The autocorrelation time estimate the number of measures of O that separate two

[1] $\sigma^2_{O(X_s)}$ is the variance of O. $\sigma^2_{O(X_s)}$ and $\langle O(X_s) \rangle$ are calculated on the sample $\{X_s\}_{s=1,\dots,n}$.

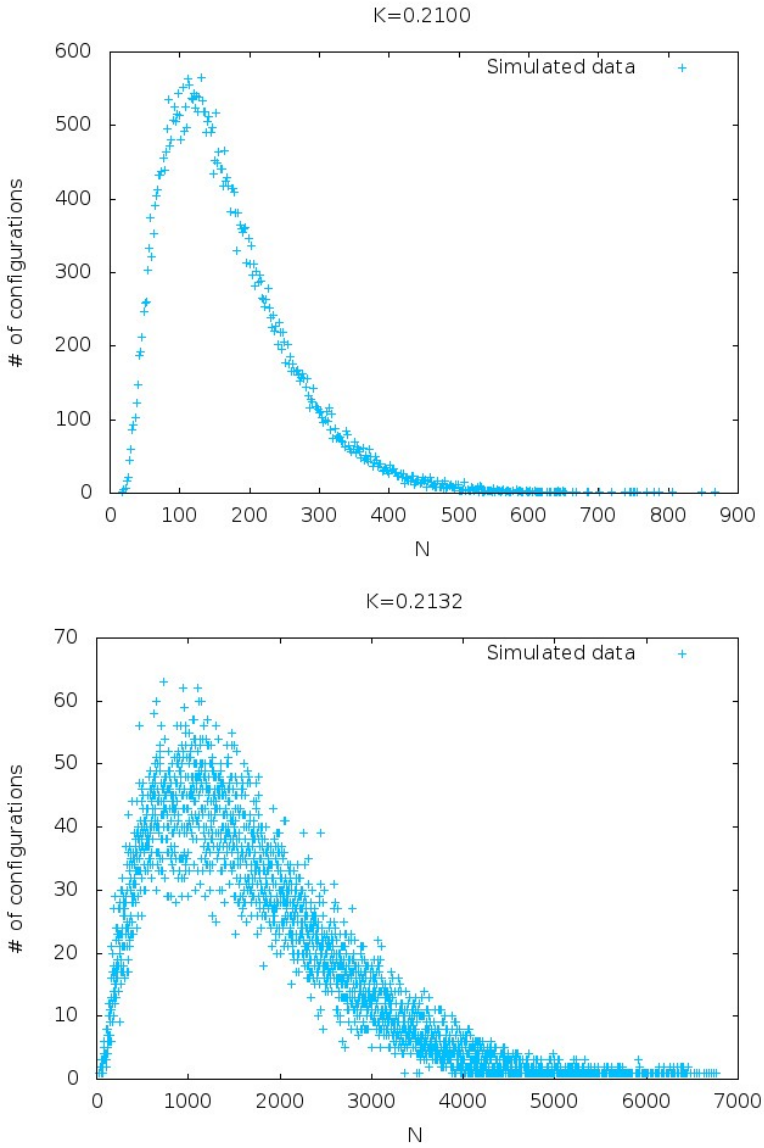

Figure 6.3: Plot of $\mathscr{Z}_N^s(\mathscr{H})$ over N for $K = 0.2100$ and $K = 0.2132$. As we approach the citical value K_c, the mean length of the configurations sampled becomes larger, but so become also the fluctuations. To improve the statistic, one can increase the number of BFACF iterations attempted or step away from K_c, sacrificing some length in the process.

independent ones and is given by

$$\tau_{int,O} = \frac{1}{2} \sum_{t=-n}^{n} f_O(t) \tag{6.3}$$

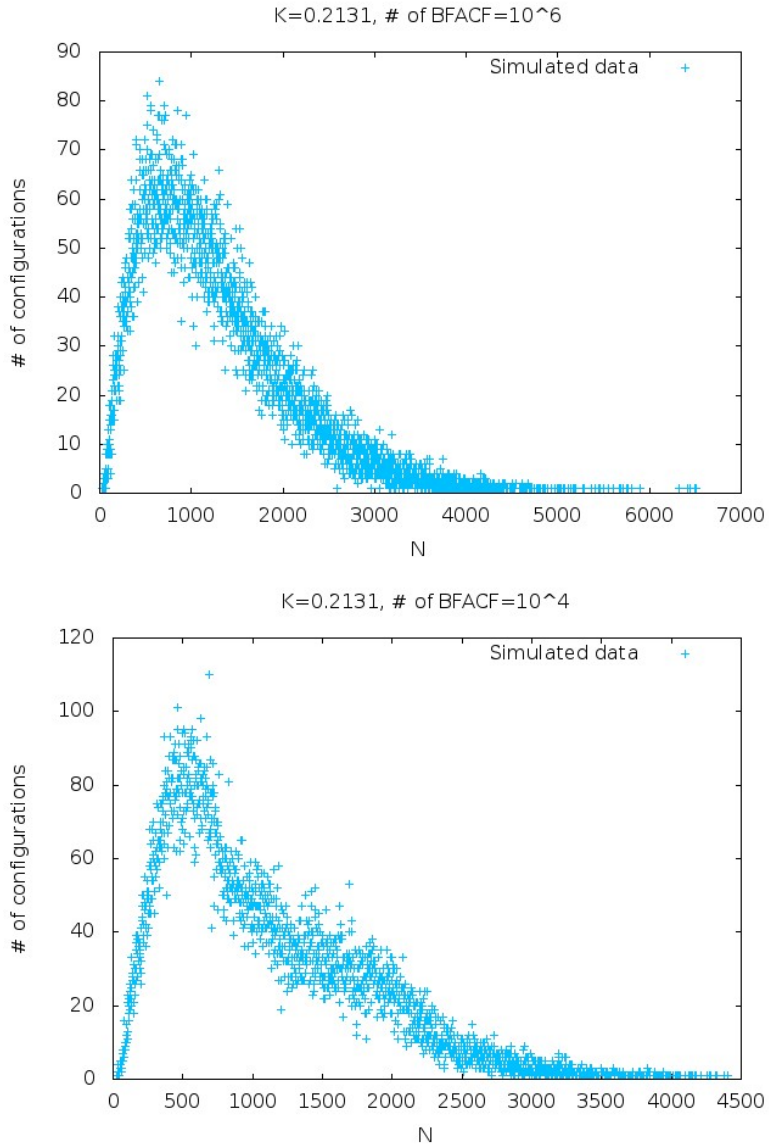

Figure 6.4: Plot of $\mathscr{Z}_N^s(\mathscr{H})$ over N for $K = 0.2131$ for a set number of 10^6 and 10^4 BFACF iterations between observations. We can see that the statistic improves by increasing the number of moves attempted: it is more probable that two consecutive sampled configurations are significantly different, so that the correlations decrease. Note that 10^4 is not enough for $K = 0.2131$, the correspondent plot has poor statistic: it exhibits more than one peak, hence cannot be fitted by the predicted behavior, recovered by increasing the number of BFACF iterations.

Ideally, we would like $\tau_{int,O}$ to be as small as possible and we say that out of all the n measures of O, only $\frac{N}{2\tau_{int,N}}$ are independent.
It is then clear that a compromise has to be made: K should be close enough to K_c to sample sufficiently long polygon pairs, but not so much that the fluctuations compromise the statistic. Our choice for the 8 chains was: $K_1 = 0.2050$, $K_2 = 0.2100$, $K_3 = 0.2120$, $K_4 = 0.2125$, $K_5 = 0.2127$, $K_6 = 0.2130$, $K_7 = 0.2131$ and $K_8 = 0.2132$.
From equation 6.2, we can also see that larger values of q biases the sampling towards configurations with larger N. By following previous studies [1], in this work we selected $q = 3$.
In table 6.1, we show the estimates of $\langle N \rangle$ and $\tau_{int,N}$ for the 8 chains, through which we can monitor how the average length of the sampled configurations and their autocorrelation times vary as K approaches the critical value.

K	$\langle N \rangle$	$\tau_{int,N}$
0.2050	82.92 ± 0.18	0.5140 ± 0.0086
0.2100	166.71 ± 0.46	0.641 ± 0.018
0.2120	350.8 ± 1.7	1.615 ± 0.096
0.2125	514.0 ± 4.2	4.19 ± 0.38
0.2127	635.3 ± 7.4	8.3 ± 1.2
0.2130	1004 ± 24	33.8 ± 7.6
0.2131	1245 ± 42	70 ± 18
0.2132	1628 ± 94	218 ± 70

Table 6.1: Mean length values and length correlation times for the 8 values of the step fugacity K. $\tau_{int,N}$ is expressed in units of sampling time interval.

6.2 Calculation of μ

Let us start our analysis by estimating the coefficient μ and comparing it to the Guttmann estimate.
Let us consider equation 6.2: we can rewrite it, after the substitution $q = 3$, as

$$\begin{aligned} \frac{1}{\langle N \rangle (K, \mathscr{H})} &\approx \frac{1}{a(\mathscr{H})\mu K} - \frac{1}{a(\mathscr{H})}, \\ a(\mathscr{H}) &= \gamma_{\mathscr{H}} + 3. \end{aligned} \tag{6.4}$$

$\langle N \rangle^{-1}$ is zero when $K = \mu^{-1}$, so we can get μ by a linear regression of $\langle N \rangle^{-1}$ over K^{-1} and extrapolating the value for which the fitting function $f(K^{-1}) = a + b \cdot K^{-1}$

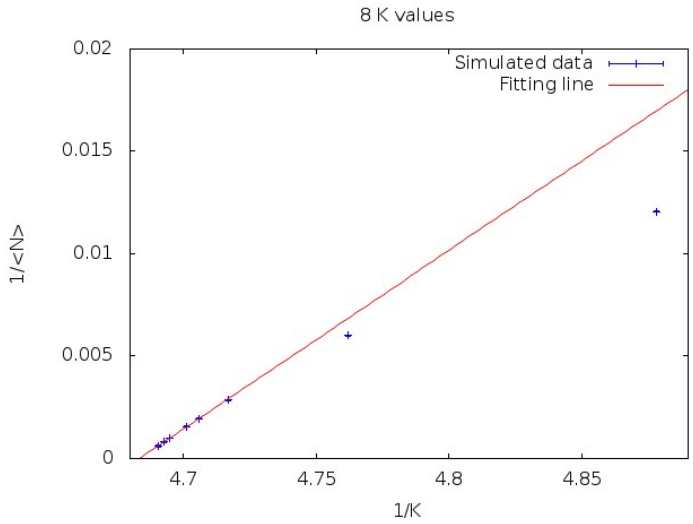

Figure 6.5: Plot of $\langle N \rangle^{-1}$ over K^{-1} for all the 8 values of K. The points corresponding to the highest values of K^{-1} exhibit a deviation from the linear behavior: we are using asymptotic relations, so the region they describe is the one near K_c. The fit function goes to zero when $K^{-1} = \mu$, as a consequence we can extract the value of μ from the fitting parameters.

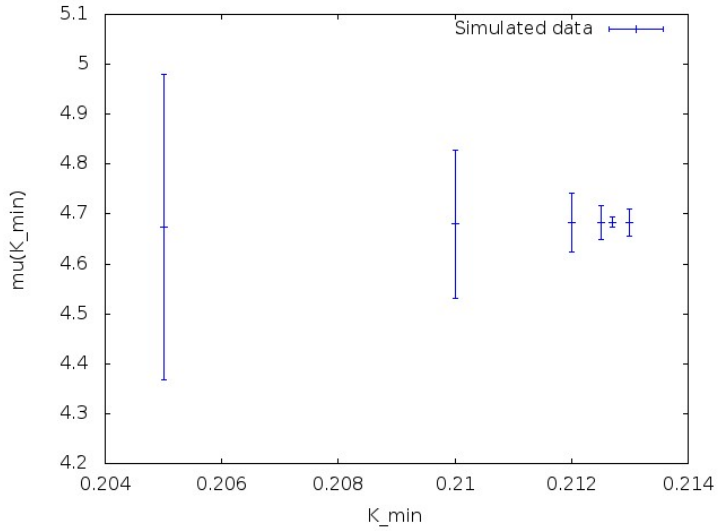

Figure 6.6: Plot of $\mu(K_{min})$ over K_{min}. We can see that the further away from K_c we go, the larger the error on μ becomes, hence we fit only the region $K > 0.2125$.

goes to zero: $\mu = -\frac{a}{b}$.
From the plot of $\langle N \rangle^{-1}$ over K^{-1}, found in figure 6.5, it seems that the points

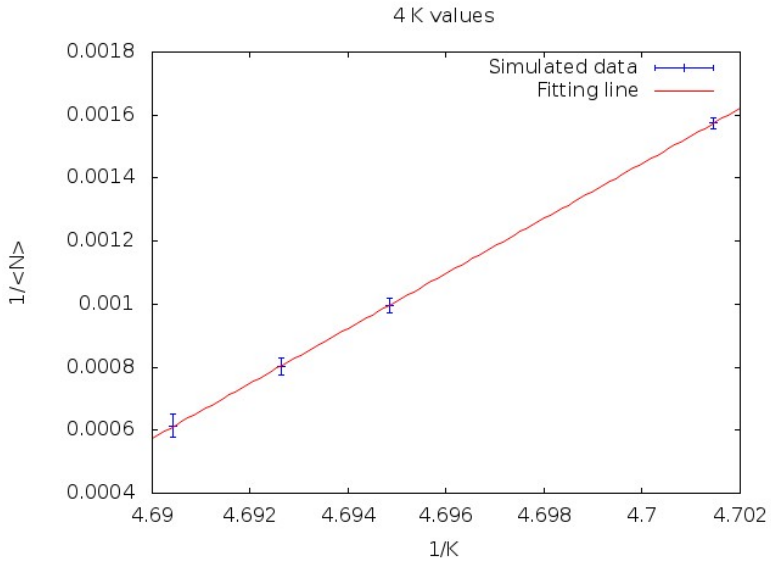

Figure 6.7: The fit of $\langle N\rangle^{-1}$ over K^{-1} performed with only the 4 highest values of K. The result is $\mu = 4.6834 \pm 0.0075$, which is compatible with the Guttmann estimate.

corresponding to the smallest values of K exhibit a deviation from the linear behavior: this is somehow expected since the relations we are using are asymptotic ones, so they are more valid the closer K is to the critical value. If we were to include in the fit values of K outside the linear region, we would expect a deviation from the value of μ obtained fitting only points inside it. We can select which points to discard by calculating μ by fitting data from a minimum value of K, K_{min}, progressively decreasing it and monitoring the value of μ.
The result of this procedure is shown in figure 6.6: the further away from K_c we go, the larger the error on μ becomes.
We propose to estimate of μ by using only the 4 highest values of K (see figure 6.7), where linearity is well satisfied. This gives

$$\mu = 4.6834 \pm 0.0075, \tag{6.5}$$

which is, indeed, within its error, compatible with the Guttmann estimate.

6.3 Calculation of $\gamma_{\mathscr{H}}$

Given μ, we can now estimate $\gamma_{\mathscr{H}}$.
We will use two methods.

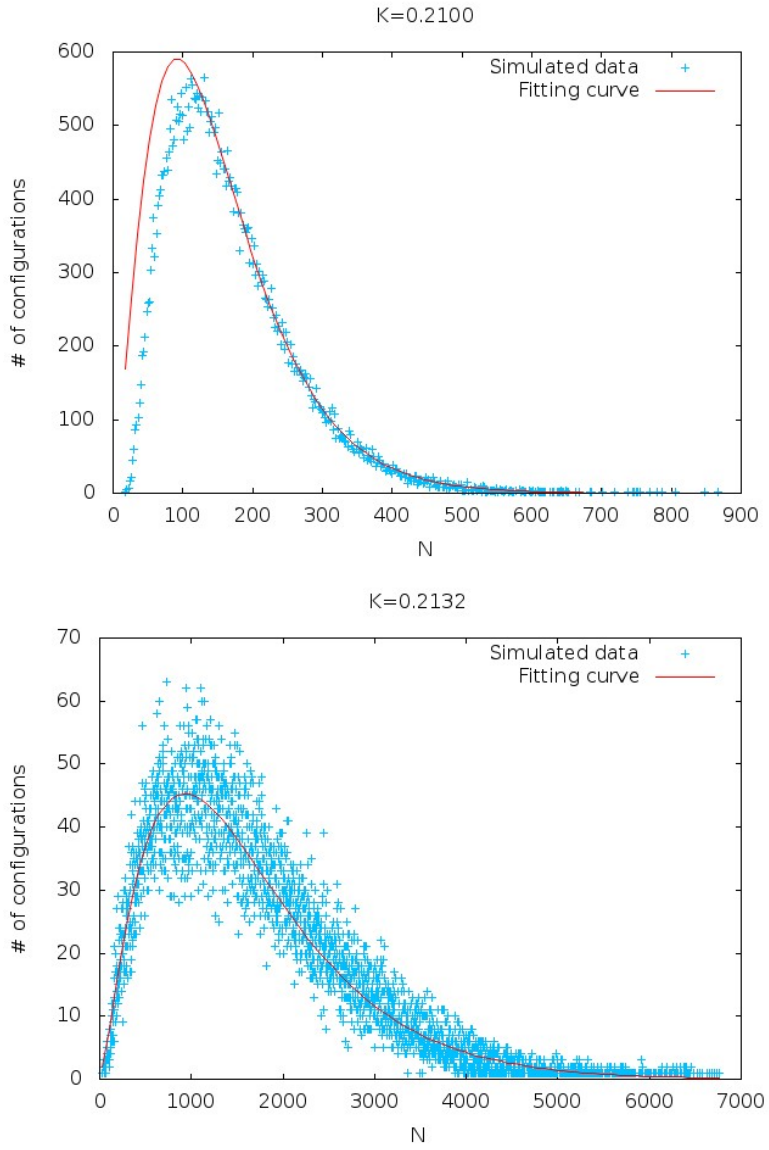

Figure 6.8: Nonlinear fit of $\mathscr{Z}_N^s(\mathscr{H})$ over N for $K = 0.2100$ and $K = 0.2132$ with the 2 parameters function $f(N) = a(\mu K)^N N^b$. From b one can extract $\gamma_{\mathscr{H}}$. Note that $f(N)$ suits well the data, but only when N is large enough, even for the selected value of K (0.2132) nearest to K_c.

- The first one directly consists in performing a nonlinear regression of $\mathscr{Z}_N^s(\mathscr{H})$ over N.
- The second is based on the linearization of equation 6.1.

6.3.1 Nonlinear regression

The predicted scaling is

$$\mathscr{Z}_N^s(\mathscr{H}) \approx AN^{2+\gamma_{\mathscr{H}}}(\mu K)^N, \tag{6.1}$$

where A is a suitable amplitude. We could try to compare this expression to our data by performing a χ^2 test, using the values we predicted for γ; the problem is that we don't know A: using the theory of appendix A, we can calculate an approximation of the amplitude for a given network topology, however for the Hopf link topology we would need also an exact value for the additional configuration factor we discussed in chapter 3.
What we can do is to fit $\mathscr{Z}_N^s(\mathscr{H})$ with the function $f(N) = a(\mu K)^N N^b$ for every value of K. As we discussed in the previous section, we can use the Guttmann estimate of μ, so we are left with only two fitting parameters, a and b, with $\gamma_{\mathscr{H}} = b-2$. We know that we should consider only long configurations. As a consequence, we need to select an appropriate fit range, $[N_{min}, N_{max}]$ for every value of K. How we can achieve this (for both methods of estimating $\gamma_{\mathscr{H}}$) is explained in the next section.
From figure 6.8, it is clear that, especially for smaller values of K (smaller configurations are involved), the performed fits do not represent very well the data corresponding to small values of N: this is not surprising, remembering that equation 6.1 is valid asymptotically. Anyway, for the selected number of BFACF iterations, the chosen values of K and larger lengths, the data seems to distribute according to the expected behavior, described by $f(N)$. In table 6.2 we report the estimates. It seems (figure 6.9) that for small values of K the more we approach the critical

K	$\gamma_{\mathscr{H}}$
0.2050	-0.250 ± 0.044
0.2100	-0.482 ± 0.022
0.2120	-0.561 ± 0.018
0.2125	-0.681 ± 0.023
0.2127	-0.672 ± 0.020
0.2130	-0.738 ± 0.019
0.2131	-0.733 ± 0.017
0.2132	-0.707 ± 0.023

Table 6.2: Values of $\gamma_{\mathscr{H}}$ obtained by nonlinear regression for every value of the step fugacity K.

point the more negative $\gamma_{\mathscr{H}}$ gets, until it stabilize from $K = 0.2130$ (further investigation near the critical point should be required, however). This agrees with

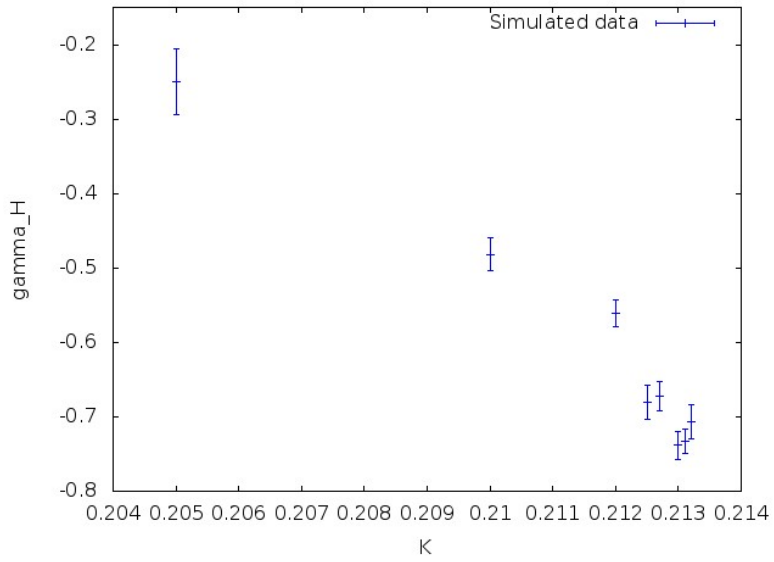

Figure 6.9: Moving toward K_c, $\gamma_{\mathscr{H}}$ become more negative, until $K = 0.2130$ is reached. We propose, as our estimate, the mean value of the last 3: $\gamma_{\mathscr{H}} = -0.727 \pm 0.011$.

the deviation from the predicted behavior we observed for small values of K when estimating μ.
Since the values of $\gamma_{\mathscr{H}}$ obtained for $K = 0.2130$, $K = 0.2131$ and $K = 0.2132$ are compatible with each other, we propose as the estimate of $\gamma_{\mathscr{H}}$ based on this method

$$\gamma_{\mathscr{H}} = -0.727 \pm 0.011. \tag{6.6}$$

6.3.2 Linear regression

An estimate of $\gamma_{\mathscr{H}}$ can be also obtained by taking the logarithm of equation 6.1,

$$\ln(\mathscr{Z}_N^s(\mathscr{H})) = (\gamma_{\mathscr{H}} + 2)\ln(N) + N\ln(\mu K) + C, \tag{6.7}$$

and perform a linear regression (C is a suitable constant). If we subtract the known linear term (we can use the Guttmann value of μ) $N\ln(\mu K)$ to $\ln(\mathscr{Z}_N^s(\mathscr{H}))$ and linearly fit the result over $\ln(N)$, we get a straight line with slope, b, related to the exponent by $\gamma_{\mathscr{H}} = b - 2$.
As we can see from the examples of figure 6.10, for small values of N there is a deviation from the linear behavior; as before, we need to select an appropriate fit region $[N_{min}, N_{max}]$. We achieved this through the same method we used for the estimate of μ. For every value of K, we computed $\gamma_{\mathscr{H}}(N_{min}, N_{max})$, by starting

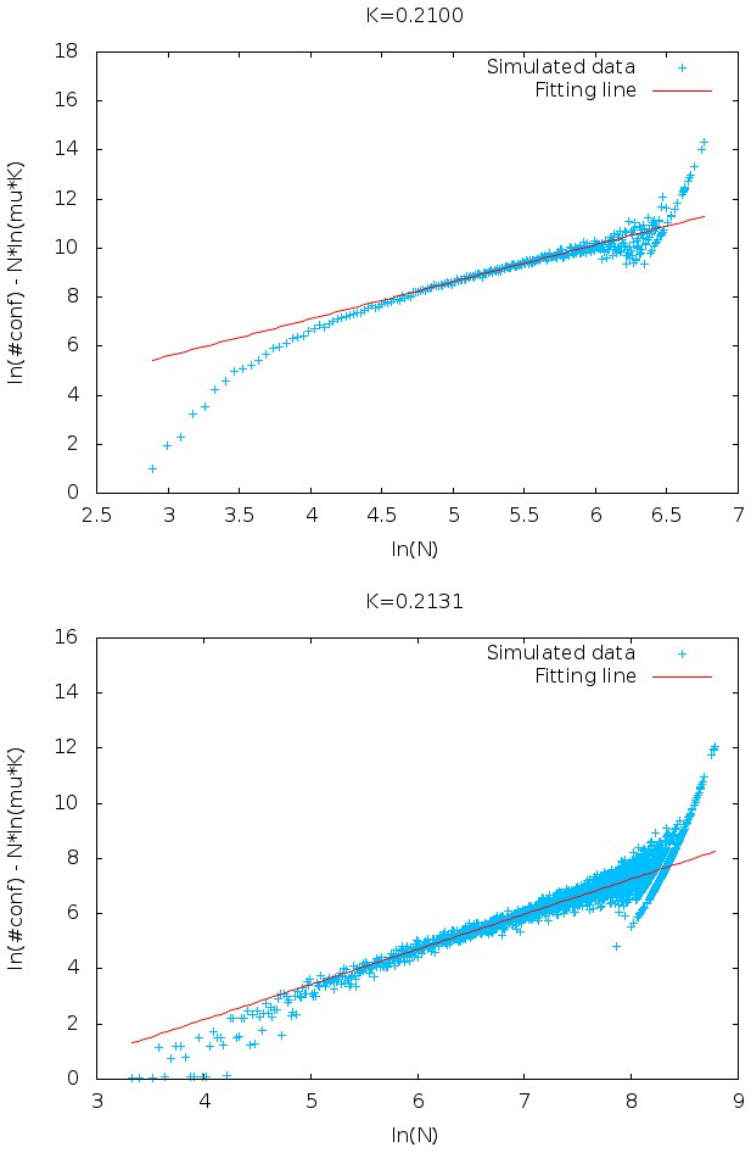

Figure 6.10: Linear fit of $\ln(\mathscr{Z}_N^s(\mathscr{H})) - N\ln(\mu K)$ over $\ln(N)$ for $K = 0.2100$ and $K = 0.2131$. From the slope of the fitting line, we can extract $\gamma_{\mathscr{H}}$.

from a small regression region, centered in the area displaying linear behavior and enlarging it up until considerable deviations from the initial one appeared in the value of $\gamma_{\mathscr{H}}(N_{min}, N_{max})$. In figure 6.11, we can see a couple of examples of what we obtained when varying N_{min} with a fixed N_{max}. Table 6.3 collects the results thus obtained.
We can make analogous considerations about the plot $\gamma_{\mathscr{H}}$ vs K (figure 6.12) as

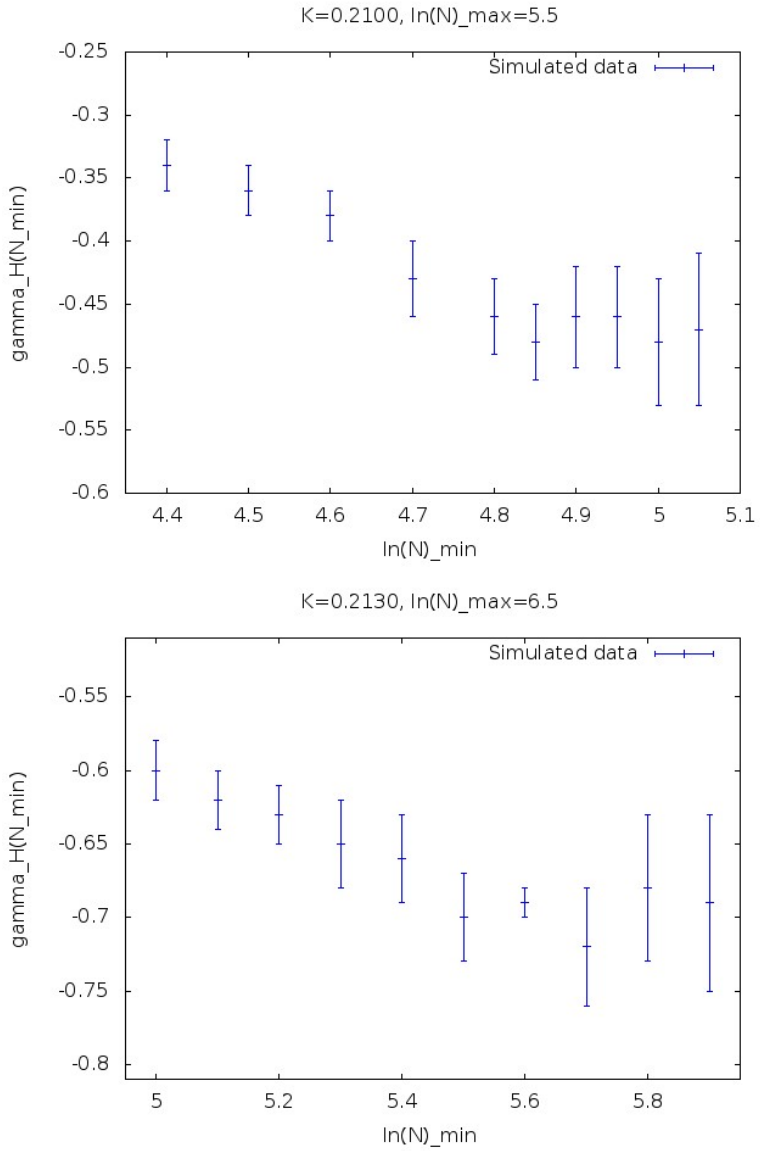

Figure 6.11: Plot of $\gamma_{\mathscr{H}}(N_{min}, N_{max})$ over $\ln(N_{min})$ (with fixed N_{max}) for $K = 2100$ and $K = 2130$. Deviations from the expected behavior emerge when N_{min} is small: we should not extend too much the fit region.

those of the previous section.
Hence, we can take as estimate of $\gamma_{\mathscr{H}}$ based on this method

$$\gamma_{\mathscr{H}} = -0.727 \pm 0.011, \tag{6.8}$$

that is very close to the one obtained by non linear regression.

K	$\gamma_{\mathscr{H}}$
0.2050	-0.337 ± 0.038
0.2100	-0.485 ± 0.022
0.2120	-0.581 ± 0.018
0.2125	-0.689 ± 0.024
0.2127	-0.676 ± 0.020
0.2130	-0.739± 0.019
0.2131	-0.726 ± 0.016
0.2132	-0.717 ± 0.022

Table 6.3: Values of $\gamma_{\mathscr{H}}$ obtained by linear regression for every value of K.

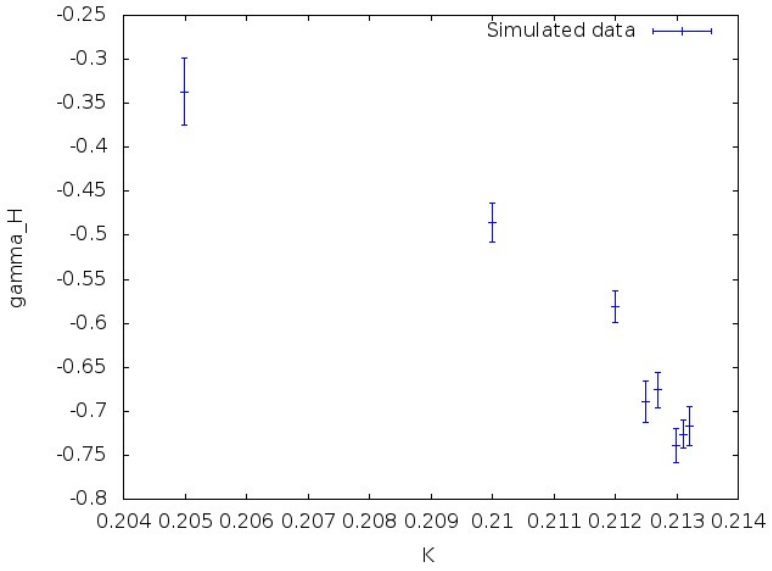

Figure 6.12: Plot of $\gamma_{\mathscr{H}}$ over K. We can take, as estimate of $\gamma_{\mathscr{H}}$, the mean value of these obtained with the 3 highest K: $\gamma_{\mathscr{H}} = -0.727 \pm 0.011$.

6.4 Remarks

How do these values of the exponent $\gamma_{\mathscr{H}}$ compare with those predicted in chapter 3?
To answer this question, let us first specify how precise the predicted values are. The calculations of exponents for networks in d dimensions in Duplantier's theory are approximations up to some order of $\epsilon = 4 - d$. We are considering networks on the cubic lattice, hence $\epsilon = 1$ is not exactly a small perturbation parameter. Going back to chapter 3, one can see how the terms of the second and third order in ϵ contributing to the theoretical expected values of $\gamma_{\mathscr{H}}$ are not much smaller than

the first order ones: we can expect corrections at the first decimal place on those predictions[2]. This reflects on the values calculated for $\gamma_{\mathscr{H}}$ of the monodisperse Hopf links with localized or delocalized linked region, which were obtained by association with networks.
On the other hand, the estimate of $\gamma_{\mathscr{H}}$ for the polydisperse case is accurate up to the third decimal place: it is 1 plus the exponent of unknotted single loops, which is -1.763 ± 0.003 ($\alpha(\emptyset) \approx \alpha$) [6].
We should also remember that the configurations with a two point linked portion (see figure 6.1(c)) are a fraction of all the ones with delocalized linked region. If we assume, for example, that the number of all the delocalized configurations is greater than that of the two point ones by a factor N^{α}, for some $\alpha \in \mathbb{R}^{+}$, then we expect an exponent associated to them greater of the two point one by α.
Our result is $\gamma_{\mathscr{H}} = -0.727 \pm 0.011$. As we pointed out, the predicted values for the two monodisperse cases are not extremely accurate, but the difference between this result and the expected ones is nearly one unit for the delocalized linked region case and only at the second decimal place for the localized linked region case. This is a strong indication that in the asymptotic limit the linked portion of an Hopf link grows as $\mathcal{O}(N)$.
Can we conclude if monodisperse or polydisperse configurations are favored?
The prediction on the monodisperse case exponent, $\gamma_{\mathscr{H}} = -0.748$, is deemed to be affected by errors up to the first decimal place, while the one on the polydesperse case, $\gamma_{\mathscr{H}} = -0.763$, only up to the third decimal place. Given how the simulation result differs from these up to second decimal place, we are lead to believe that the winning scenario is the second one: not only the liked region grows as $\mathcal{O}(N)$, but one of the two loops does to.
To verify this statement, we can check how the lengths of the two loops of the configurations we sampled compare to each other. In figure 6.13, we plotted the last configuration sampled for every value of K: we, indeed, observe that one of the two loops is significantly smaller than the other and this is more evident as we increase (K) the total length N. Note that, especially from their XY projections of figure 6.14, it also seems that the linked region of these configurations is more localized than not. To take into account all the sampled configurations, we propose, as estimate of the mean polydispertion ratio, the coefficient $P = \langle \frac{|N_1 - N_2|}{N} \rangle$, where N_1 and N_2 are the lengths of the two loops and $N = N_1 + N_2$ the total length. In table[3] 6.4, we can see how P grows as $\langle N \rangle$ becomes larger. Note that complete polydispertion is represented by $P = 1$ and for $K = 0.2132$, $P \sim 0.8$. This suggests that we should move even further toward the critical value K_c to reach the asymptotic limit and in doing so possibly $\gamma_{\mathscr{H}}$ could converge even more exactly

[2]Se the numbers in chapter 3.
[3]Correlations were not taken into account in the calculation of σ_P.

to the expected value.

K	P
0.2050	0.3732 ± 0.0010
0.2100	0.4882 ± 0.0012
0.2120	0.6008 ± 0.0012
0.2125	0.6548 ± 0.0012
0.2127	0.6818 ± 0.0012
0.2130	0.7373± 0.0012
0.2131	0.7618 ± 0.0011
0.2132	07856 ± 0.0011

Table 6.4: Values of P obtained for every value of K.

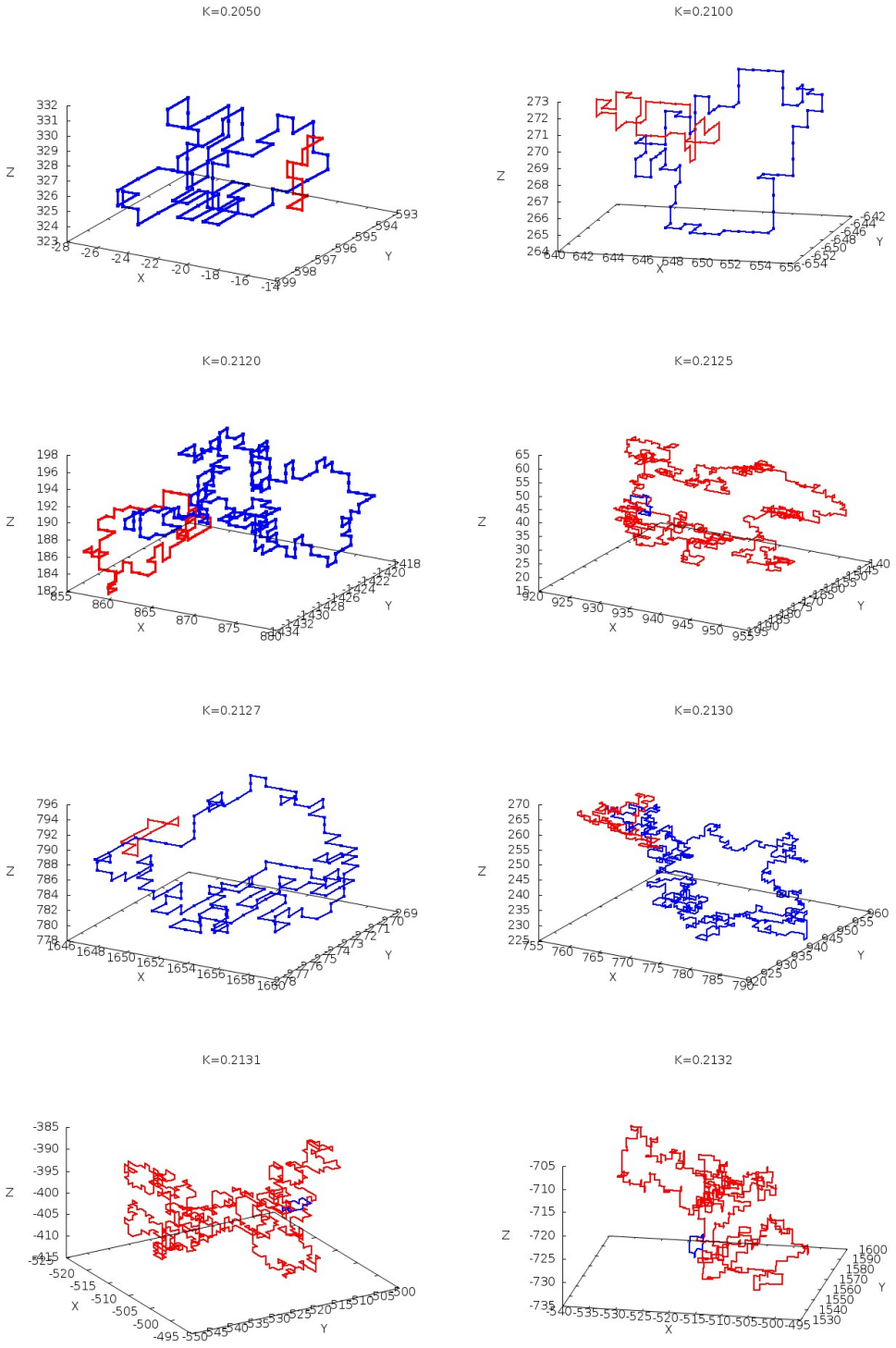

Figure 6.13: Examples of configurations sampled for every value of K. We can see that one of the two loops is significantly smaller than the other. Moreover, it seems that the linked region of these configurations is localized and there is no clear evidence of two points linked portions (see also figure 6.14).

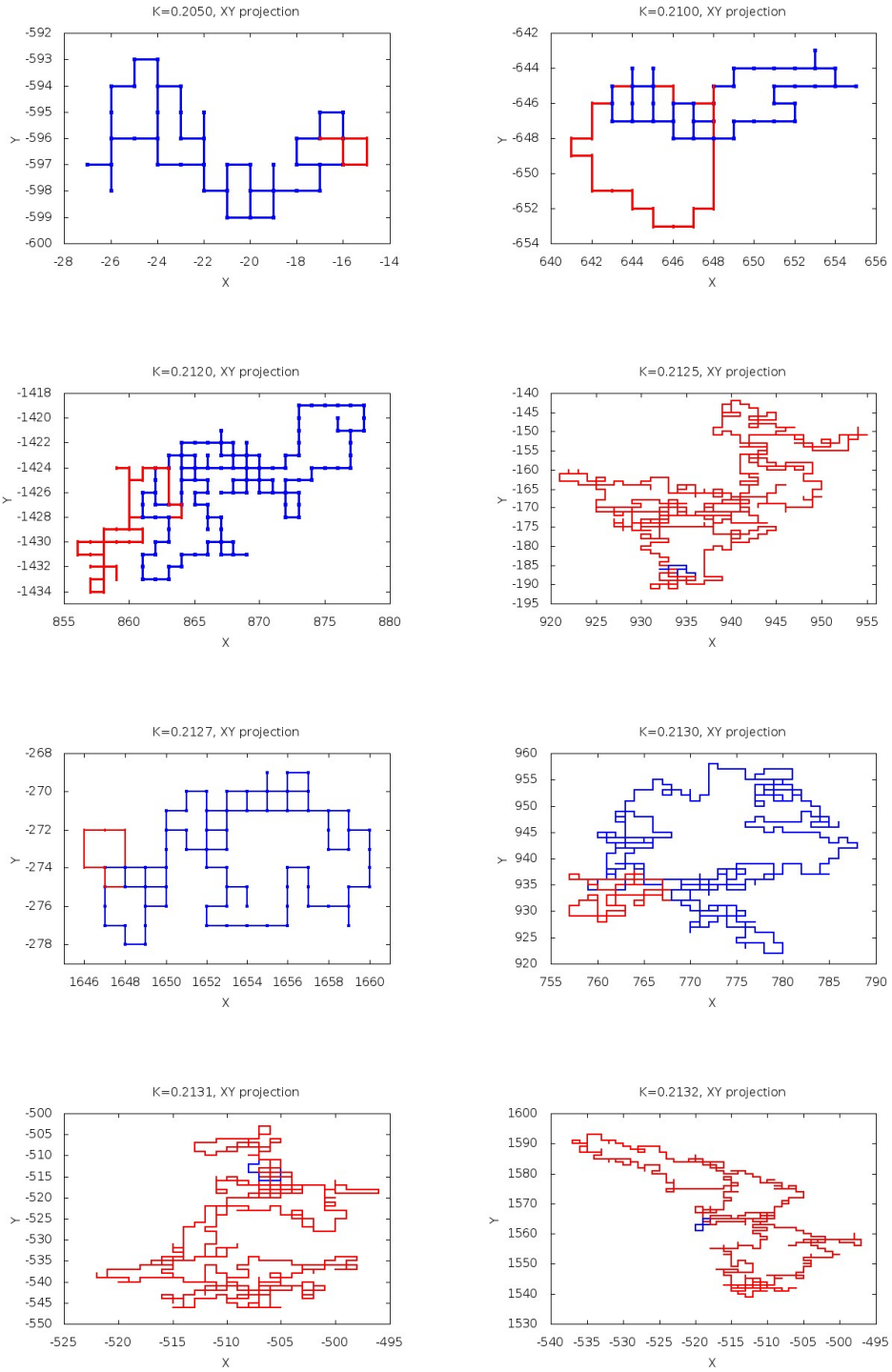

Figure 6.14: Projections on the plane XY of the configurations of figure 6.13.

Chapter 7

Conclusions

The purpose of this work was to understand if the number of asymptotic configurations of links with the Hopf topology, $\mathscr{H}$, could be described by the scaling law of networks, namely

$$\mathscr{Z}_N(\mathscr{H}) \sim \mu^N N^{\gamma_{\mathscr{H}}-1} \qquad (N \gg 1), \tag{3.1}$$

where $\mathscr{Z}_N(\mathscr{H})$ is the number of configurations with total length N and topology $\mathscr{H}$, and if the linked region, in the large lengths limit, becomes localized or not.
In chapter 3, we discussed that we can, in the asymptotic limit, associate

- an eight-like network to a monodisperse Hopf link with localized linked region (figure 7.1(a));
- a watermelon network with 4 legs to a monodisperse Hopf link with delocalized linked portion and two contact points (figure 7.1(b)) and
- a loop with a point to a polydisperse Hopf link (figure 7.1(c)).

Moreover, we predicted $\mu = 4.68393 \pm 0.00002$ (Guttmann estimate) and $\gamma_{\mathscr{H}} = -0.748$ for the first case, $\gamma_{\mathscr{H}} = 0.044$, for the second case and $\gamma_{\mathscr{H}} = -0.763$ for the third case; we also pointed out that the first two estimate of $\gamma_{\mathscr{H}}$ are deemed to be affected by errors up to the first decimal place, while the third only up to the third decimal place.
In chapter 4, we showed that we can extend the BFACF algorithm for polygons on the cubic lattice to any number of linked polygons in $\mathbb{Z}^3$ and, in chapter 5, we showed that the ergodicity classes of this extension are made of all and only links of the same arbitrary but fixed topology.
Using these results, in chapter 6, we were able to simulate configurations with the Hopf topology with lengths up to the order 10^3, and to estimate $\mu = 4.6834 \pm 0.0075$, which is compatible with the predicted value, and $\gamma_{\mathscr{H}} = -0.727 \pm 0.011$.

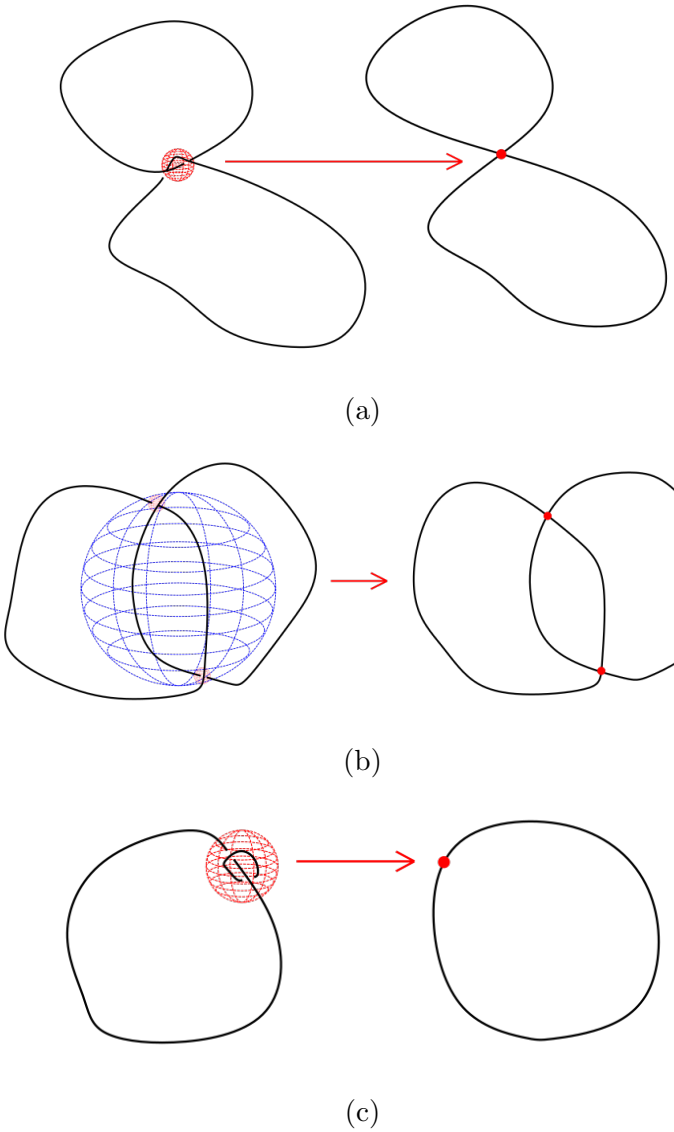

Figure 7.1: **(a)** Monodisperse Hopf link with localized linked portion: in the asymptotic limit it can be described by an eight-like network. **(b)** Monodisperse Hopf link with delocalized linked portion and two contact points. In the large lengths limit it can be described by a watermelon network with 4 legs. **(c)** A polydisperse Hopf link can be associated, in the asymptotic limit, to a loop with a point.

As we discussed, we believe that the simulation results are an indication that equation 3.1 can indeed be used to describe the asymptotic behavior of the Hopf

links and that, taking also into account the estimated values of the coefficient $P = \langle \frac{|N_1 - N_2|}{N} \rangle$, in the large lengths limit Hopf configurations are predominantly polydisperse.
The obtained estimate of $\gamma_{\mathscr{H}}$ does not exactly coincide, even though the difference is only up to the second decimal place, with the predicted one for the polydisperse case; however, by moving towards the critical point, hence larger configurations, we think this difference might cancel. Note that in order to achieve this, one should perform a simulation with increased statistic (i.e. with an increased total number of attempted BFACF moves).
The ideas and results contained in the first 5 chapters of this work are general: the procedure applied to study the Hopf topology can be extended to any fixed topology for any number of linked loops, at the eventual cost of calculating new suitable exponents associated with networks different from the eight-like and the watermelon ones.
By doing this, we could investigate if every topology of a couple of linked loops (e.g. the Solomon one, illustrated in figure 7.2) is dominated, in the asymptotic limit, by polydisperse configurations, and we could also study the behavior of links made by more than two loops.
Let us give 3 examples:

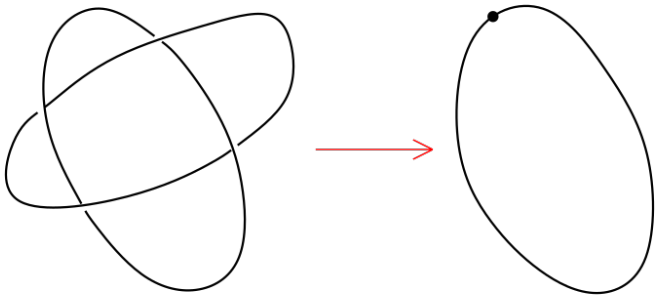

Figure 7.2: An example of Solomon link. Are asymptotic configurations with the Solomon topology predominantly polydisperse, like the Hopf ones, or are they better associated with some network topology?

1. can a chain made by 3 unknotted linked loops with Hopf-like linked regions be described by the eight-like networks, like illustrated in figure 7.3?

2. Is the Borromean ring of figure 7.4 described by a watermelon network in the large lengths limit?

3. can a ring of an arbitrary number of unknotted linked loops with Hopf-like

linked portions be associated with a single loop with a point in the asymptotic limit, like shown in figure 7.5?

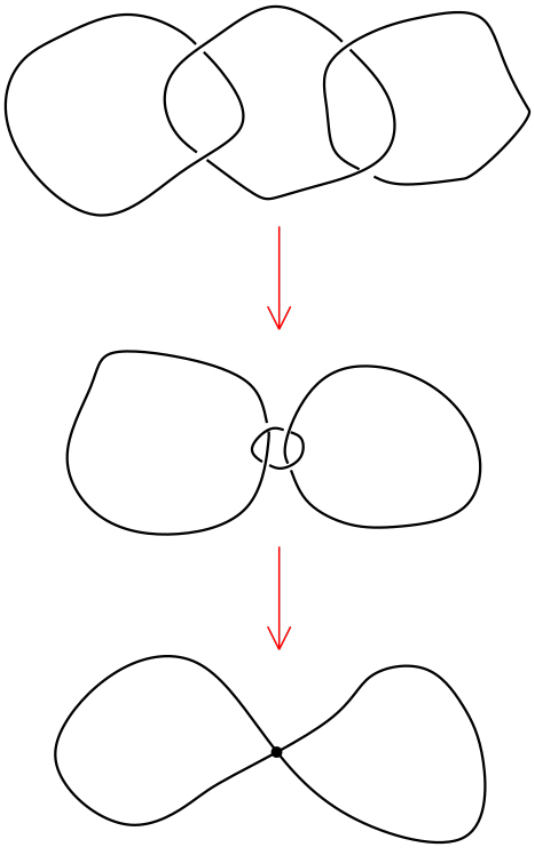

Figure 7.3: If we call N the total length of a chain made of 3 unknotted linked loops with Hopf-like linked regions, and if in the large N limit the central loop grows as $o(N)$, while the others as $\mathcal{O}(N)$, then this link can be described by an eight-like network.

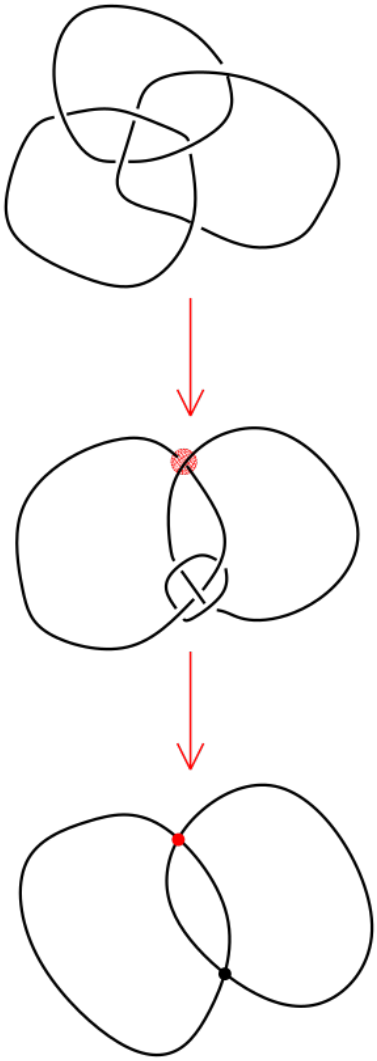

Figure 7.4: Let us call N the total length of a Borromean ring, the one shown at the top of this figure. If in the asymptotic limit one of the 3 loops grows as $o(N)$ and if there is a contact point like shown in the central picture, then this link can be described by a watermelon network with 4 legs.

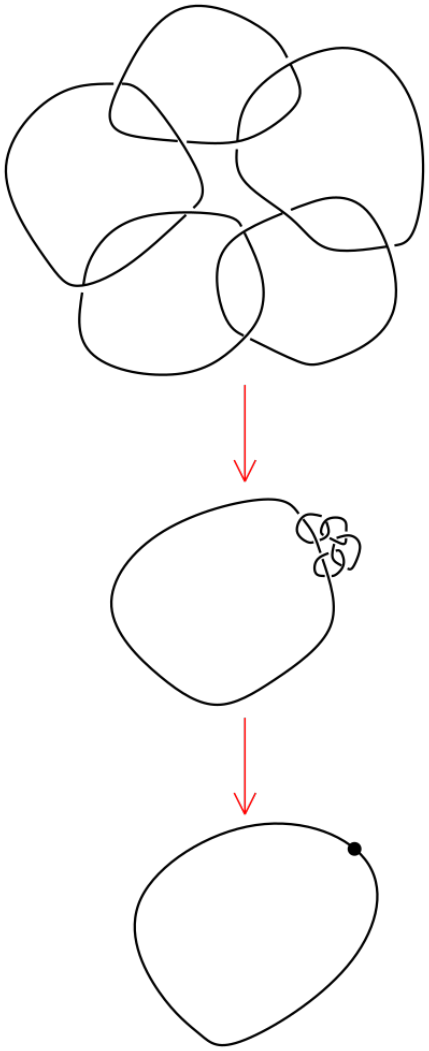

Figure 7.5: If all the loops except one of a ring of unknotted linked loops with Hopf-like linked portions grow as $o(N)$ in the large lengths limit (N is the total length of the ring), then the link can be associated with a single loop with a point.

Appendix A

First Order Perturbation Expansion of the Partition Function of the Watermelon and the Eight-Like Networks

It is instructive to use the direct theory of polymers to expand the partition functions of the networks we used in our work in powers of the parameters b and ϵ. In this way, not only we can test by hand the insurgence of ultra-violet divergences and how one can factorize out the scaling contribution of loops, but also understand the details of how one can calculate an approximation of the critical exponents σ_L and the amplitude $\mathscr{A}$.

A.1 Generic rules

Let us remember that in chapter 2 we stated that the partition function of any given network topology $\mathscr{G}$ in $\mathbb{R}^d$, $\mathscr{Z}(\mathscr{G})$, is given by

$$\begin{aligned}
\mathscr{Z}(\mathscr{G}) &= \frac{\int \prod_{a=1}^{\mathscr{N}} d\{\vec{r}_a\}\delta^d[\mathscr{G}]\mathscr{P}_{\mathscr{N}}\{\vec{r}_a\}}{\Big[\int d\{\vec{r}\}P_0\{\vec{r}\}\delta^d(\vec{r}(0))\Big]^{\mathscr{N}}},\\
\mathscr{P}_{\mathscr{N}}\{\vec{r}_a\} &= \exp\Big[-\frac{1}{2}\sum_{a=1}^{\mathscr{N}}\int_0^S \Big(\frac{d\vec{r}_a(s)}{ds}\Big)^2 ds\\
&\quad -\frac{1}{2}b\sum_{a=1}^{\mathscr{N}}\sum_{a'=1}^{\mathscr{N}}\int_0^S ds\int_0^S ds'\delta^d(\vec{r}_a(s)-\vec{r}_{a'}(s'))\Big]\\
\delta^d[\mathscr{G}] &= \int\prod_{i=1}^{\mathscr{V}-1} d^d\vec{R}_i\prod_{i=1}^{\mathscr{V}}\Big[\prod_{a\in L^+(i)}\delta^d(\vec{r}_a(0)-\vec{R}_i)\prod_{a'\in L^-(i)}\delta^d(\vec{r}_{a'}(S)-\vec{R}_i)\Big].
\end{aligned} \tag{2.18}$$

We invite the reader to refer to chapter 2 for the understanding of this expression. In order to write this function as a series of powers of b, we need to expand $\mathscr{P}_{\mathscr{N}}$ and Furier-transform each δ in both $\mathscr{P}_{\mathscr{N}}$ and $\delta^d[\mathscr{G}]$.
We are giving the rules to calculate each order [2]. Each order is associated with a number of diagrams.

1. We construct a bare diagram structure at any order by associating a continuous line to each of the chains building $\mathscr{G}$, and connect them, respecting the topology, to dots representing the vertices.

2. Diagrams of the n^{th} order are obtained by connecting n couples of points of the bare structure with dotted lines. We call these points interaction points.

3. Given a diagram, we identify a complete set of independent loops, considering both the continuous and the dotted lines[1] and assign a momentum $\vec{q}_i$, $i = 1,\ldots,\mathscr{L}$ flowing through each of them.

4. Each diagram of the n^{th} order contributes with a term given by integration, with measure
$$\int\int\Big[\prod_{a=1}^{n} d^d\vec{x}_{1,a}d^d\vec{x}_{2,a}\Big]\int\prod_{i=1}^{\mathscr{L}}\frac{d^d\vec{q}_i}{(2\pi)^d},$$
where the first two integrals are over all possible positions of interaction points that preserve the interaction topology, of the product of

[1] The number of these loops is given by Euler's formula 2.5.

- a factor $-b$ for each interaction line;
- a factor $\exp[-\frac{1}{2}(\sum \vec{q})^2 s]$ for each segment of length s of the network. The sum is intended as over all the momenta flowing through the segment.

5. For the total n^{th} order term, one has to sum over all contributions associated with said order diagrams.

We will see, in the next section, that, in order to avoid the insurgence of divergences, we actually need to add a rule to these [12].

A.2 Zeroth and first order calculations for the eight-like networks

Now that we know the rules, we can try to compute the first order contribution to the partition function of the two network types we worked on.
Generally speaking, we can perform calculations with branches of different lengths S_i, $i = 1, \ldots$. Eventually, we can always restrict ourselves to $S = S_1 = S_2 = \ldots$, if the results are of impractical use (we are interested in the monodisperse case, anyway). We start from the network topology associated, in the asymptotic limit, to two unknotted loops with localized linked region, i.e. the eight-like one, $\mathscr{G}_1$. We will be discussing the generic d dimensional case.

Zeroth order For the zeroth order, as we can tell from figure A.1, we have two independent loops, with momenta $\vec{q}_1$ and $\vec{q}_2$ and we don't have any dotted line; the associated contribution reads

$$\mathscr{Z}_0(\mathscr{G}_1) = \int \frac{d^d\vec{q}_1}{(2\pi)^d} \int \frac{d^d\vec{q}_2}{(2\pi)^d} e^{-\frac{1}{2}q_1^2 S_1} e^{-\frac{1}{2}q_2^2 S_2}. \tag{A.1}$$

This is a simple gaussian integral, so remembering

$$\int d^d\vec{x} e^{-\frac{1}{2}x^2\alpha - \vec{v}\vec{x}} = \alpha^{-\frac{d}{2}} (2\pi)^{\frac{d}{2}} e^{\frac{v^2}{2\alpha}}, \tag{A.2}$$

we get

$$\mathscr{Z}_0(\mathscr{G}_1) = \left[(2\pi)^2 S_1 S_2\right]^{-\frac{d}{2}}. \tag{A.3}$$

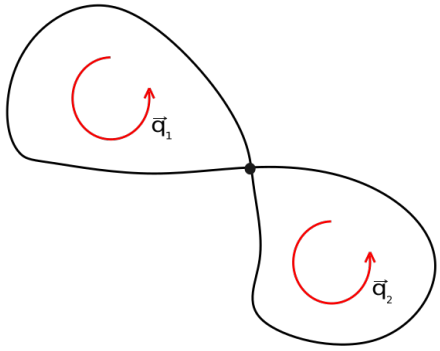

Figure A.1: The eight-like network topology; it coincides with the bare structure of its associated perturbation diagrams. When calculating the zeroth order, we don't have any dotted line and only two independent loops with their respective momenta. Note that the direction of the flow of the momenta is conventional.

First order, type A diagrams As far as the first order is concerned, we have two types of topological independent diagrams: the first one, A, is obtained connecting, with an interaction line, two points of the same chain. We can consider only the diagram with both interaction dots on one of the two branches, say the one with length S_1, and then sum to its contribution one that is obtained switching S_1 with S_2.

- We must consider all the points of the first chain, so we need do integrate over the positions of the interaction points,
- we have 3 loops and 3 momenta, $\vec{q}_1$, $\vec{q}_2$ and $\vec{q}_3$,
- there are 3 segments: through the first one, of length S_2 , flows a momentum $\vec{q}_2$, through the second, of length $S_1 - s$, a momentum $\vec{q}_2$ and through the third one, of length s, a momentum $\vec{q}_1 - \vec{q}_3$.

Taking all this into account, the contribution associated to the diagram in figure A.2 is[2]

$$\mathscr{Z}_1^{A,1}(\mathscr{G}_1) = -b \int_0^{S_1} ds(S_1 - s) \int \frac{d^d\vec{q}_1}{(2\pi)^d} \int \frac{d^d\vec{q}_2}{(2\pi)^d} \int \frac{d^d\vec{q}_3}{(2\pi)^d} \Big[e^{-\frac{1}{2}s(\vec{q}_1-\vec{q}_3)^2} e^{-\frac{1}{2}(S_1-s)q_1^2} e^{-\frac{1}{2}S_2 q_2^2} \Big] \tag{A.4}$$

[2]That apex 1 means that we are considering the contributions with the interaction points on the first chain.

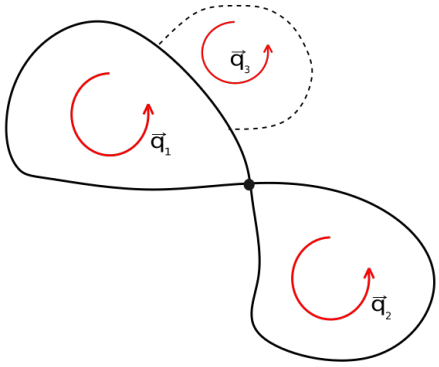

Figure A.2: First order type A diagram. This time we have one interaction line, 3 independent loops and 3 segments with different momenta flowing through them (the one delimited by the two interaction dots has two instead than only one momentum).

with the change of coordinates

$$\begin{cases} \vec{q}_1 \to \vec{q}_1 \\ \vec{q}_2 \to \vec{q}_2 \\ \vec{q}_3 \to \vec{q} = \vec{q}_1 - \vec{q}_3 \end{cases} \qquad d^d\vec{q}_1 d^d\vec{q}_2 d^d\vec{q}_3 \to d^d\vec{q}_1 d^d\vec{q}_2 d^d\vec{q},$$

we get

$$\mathscr{Z}_1^{A,1}(\mathscr{G}_1) = -b\int_0^{S_1} ds(S_1 - s)\int \frac{d^d\vec{q}_1}{(2\pi)^d}\int \frac{d^d\vec{q}_2}{(2\pi)^d}\int \frac{d^d\vec{q}}{(2\pi)^d}\Big[e^{-\frac{1}{2}sq^2}e^{-\frac{1}{2}(S_1-s)q_1^2}e^{-\frac{1}{2}S_2q_2^2}\Big]. \tag{A.5}$$

Now, if we apply equation A.2, we get

$$\begin{aligned} \mathscr{Z}_1^{A,1}(\mathscr{G}_1) &= -b\frac{1}{(2\pi)^{\frac{3}{2}d}S_2{}^{\frac{d}{2}}}\int_0^{S_1}\frac{1}{s^{\frac{d}{2}}(S_1-s)^{\frac{d}{2}-1}}ds \\ &= -b\frac{1}{(2\pi)^{\frac{3}{2}d}S_2{}^{\frac{d}{2}}}S_1^{2-d}I_1^A(\mathscr{G}_1), \end{aligned} \tag{A.6}$$

where

$$I_1^A(\mathscr{G}_1) = \int_0^1 \frac{1}{x^{\frac{d}{2}}(1-x)^{\frac{d}{2}-1}}dx.$$

Note that this is a divergent contribution for $d \geq 2$:

$$\int_0^1 \frac{1}{x^{\frac{d}{2}}(1-x)^{\frac{d}{2}-1}}dx > \int_0^1 \frac{1}{x^{\frac{d}{2}}}dx > \infty \quad (d \geq 2).$$

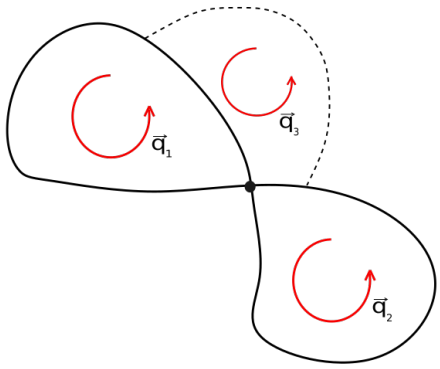

Figure A.3: First order type B diagram. This time we have 4 segments with different momenta flowing through them (the two delimited by the interaction dots and the node of the bare structure have two momenta).

First order, type B diagrams The second type of diagram, B, is made by joining two points, one for each branch with a dotted line. We have to sum over all the contributions obtained moving these points around the two chains. Using the same rules as above,

$$\mathscr{L}_1^B(\mathscr{G}_1) = -b\int_0^{S_1} ds_1 \int_0^{S_2} ds_2 \int \frac{d^d\vec{q}_1}{(2\pi)^d}\int \frac{d^d\vec{q}_2}{(2\pi)^d}\int \frac{d^d\vec{q}_3}{(2\pi)^d}\Big[e^{-\frac{1}{2}(S_1-s_1)q_1^2} e^{-\frac{1}{2}(S_2-s_2)q_2^2} e^{-\frac{1}{2}s_1(\vec{q}_1-\vec{q}_3)^2} e^{-\frac{1}{2}s_2(\vec{q}_2-\vec{q}_3)^2}\Big]. \tag{A.7}$$

This is also a gaussian integral, to solve on the momenta, we need to open up the squares at the exponents of the integrand and apply equation A.2 to integrate first on $\vec{q}_1$ and $\vec{q}_2$ and then on $\vec{q}_3$. We have

$$\begin{aligned}\mathscr{L}_1^B(\mathscr{G}_1) &= -b\frac{1}{(2\pi)^{3d}}\left(\frac{2\pi}{S_1}\right)^{\frac{d}{2}}\left(\frac{2\pi}{S_2}\right)^{\frac{d}{2}}\int_0^{S_1} ds_1\int_0^{S_2} ds_2\int d^d\vec{q}_3\left[e^{-\frac{1}{2}q_3^2\left(s_1+s_2-\frac{s_1^2}{S_1}-\frac{s_2^2}{S_2}\right)}\right]\\ &= -b\frac{1}{(2\pi)^{d\frac{3}{2}}}\frac{1}{(S_1S_2)^{\frac{d}{2}}}\int_0^{S_1} ds_1\int_0^{S_2} ds_2\left(\frac{1}{s_1+s_2-\frac{s_1^2}{S_1}-\frac{s_2^2}{S_2}}\right)^{\frac{d}{2}}\\ &= -b\frac{1}{(2\pi)^{d\frac{3}{2}}}\frac{1}{(S_1S_2)^{\frac{d}{2}}}S_1S_2I_1^B(\mathscr{G}_1),\end{aligned} \tag{A.8}$$

where

$$I_1^B(\mathscr{G}_1) = \int_0^1 dz_1\int_0^1 dz_2\left(\frac{1}{(z_1-z_1^2)S_1+(z_2-z_2^2)S_2}\right)^{\frac{d}{2}}.$$

$I_1^B(\mathscr{G}_1)$ is divergent: the integrand is always positive, and the integral on z_1 is infinite for the fixed value $z_2 = 0$ and $d \geq 2$.

These divergences are not unexpected: they are associated with the divergent contributions of contact interaction term of the Edwards partition function (the starting one, without dimension regularization). We stated that the way to deal with that is taking an ultraviolet cut-off, integrating the interaction term outside of a region $|s - s'| > s_0$, $s_o \to 0$, and that we can factorize s_0 out of the partition function, getting a dimensional regularized one.
Where the integrals we calculated diverge is at short distances between interaction points ($s \to 0$). Following [12], if we insert, in a similar way, a cut-off in $I_1^A(\mathscr{G}_1)$ and $I_1^B(\mathscr{G}_1)$; we get the sum of a regular term and a singular term dependent on a parameter $s_0 \to 0$. Summing over all the singular terms at every order, if $d < 4$, we can factorize out the dependence on s_0, as in 2.8:

$$\underset{s_0 \to 0}{\mathscr{Z}}(\mathscr{G}, b, S, s_0, d) = \exp[\mathscr{N}(S/s_0)C(z_0)]\mathscr{Z}(\mathscr{G}, b, S, d)|_{dim.reg.}.$$

In this way, we can forget about the singular terms and go on with the regular ones. Hence, we add another rule to the perturbation expansion [12].

6. An integral which is divergent at short range is replaced with its principal part. For instance, for any $n \leq -1$,

$$\int_0^1 s^n \to \lim_{s_0 \to 0} \int_{s_0}^1 s^n.$$

We can then factorize out the s_0 dependent term as said.
To proceed even further, one should Laurent-expand these regularized terms in powers of ϵ, with $d = 4 - \epsilon$, so to get a double ϵ and z expansion (up to first order in z) as in 2.25.
This is, however, as far as we go with the expansion.
We have still a last thing to discuss: from these terms we should be able to extract the scaling contribution of the loops. In chapter 2, for a monodysperse network topology, this was achieved by a dimensional analysis of the Edwards partition function; the same argument can't be applied when the branches have different lengths. Note, indeed, that the dependence on S_1 and S_2 of the first order term B is implicit and can't be extracted from $I_1^B(\mathscr{G}_1)$.
Anyway, in the asymptotic limit only the growth size matters (small differences in the lengths of the branches are not relevant). In the monodisperse case, we should recover the expected behavior by setting $S_1 = S_2 = S$ in the 3 terms we

calculated.
Remembering that $z = (2\pi)^{-\frac{d}{2}} b S^{2-\frac{d}{2}}$, up to first order, the partition function of the monodisperse eight-like networks is

$$\mathscr{Z}(\mathscr{G}_1) = S^{-d}\{A_d + zB_d + \mathcal{O}(z^2)\} \tag{A.9}$$

where A_d and B_d are functions of the dimension only.
This is as expected (equation 2.15), since the number of independent loops, $\mathscr{L}$, is 2 and $S^{-\mathscr{L}\frac{d}{2}} = S^{-d}$.

A.3 Zeroth and first order calculations for the 4-legged watermelon networks

As for the 4-legged watermelon topology, $\mathscr{G}_2$, we can directly find the zeroth and first order results in Duplantier's article [2].

Zeroth order For branches of different lengths we have

$$\mathscr{Z}_0(\mathscr{G}_2) = (2\pi)^{\frac{d}{2}} \prod_{i=1}^{4} \frac{1}{(2\pi S_i)^{\frac{d}{2}}} \Big(\sum_{i=1}^{4} \frac{1}{S_i} \Big)^{-\frac{d}{2}} \tag{A.10}$$

First order We have two different types of diagrams: the first one, A, is obtained by joining two interaction points on the same branch with a dotted line; the second one, B, by connecting two different chains.

$$\begin{aligned} \mathscr{Z}_1^A(\mathscr{G}_2) = -b(2\pi)^{-\frac{d}{2}} \sum_{i=1}^{4} \Bigg[& \prod_{j\neq i=1}^{4} (2\pi S_j)^{-\frac{d}{2}} \\ & \times \int_0^{S_i} ds (S_i - s)^{1-\frac{d}{2}} s^{-\frac{d}{2}} \Big(\frac{1}{S_i - s} + \sum_{j\neq i=1}^{4} \frac{1}{S_j} \Big)^{-\frac{d}{2}} \Bigg] \end{aligned} \tag{A.11}$$

and

$$\begin{aligned} \mathscr{Z}_1^B(\mathscr{G}_2) = -b(2\pi)^{-\frac{d}{2}} \sum_{\substack{i,j=1 \\ i\neq j}}^{4} \Bigg\{ & \int_0^{S_i} ds_1 \int_0^{S_j} ds_2 (s_1 + s_2)^{-\frac{d}{2}} (2\pi)^{-d\frac{3}{2}} \prod_{k\neq i,j}^{4} (S_k)^{-\frac{d}{2}} \\ & \times \Bigg[S_i + S_j - s_i - s_j + \Bigg(\sum_{k\neq i,j}^{4} \frac{1}{S_k} \Bigg) \Bigg(S_i S_j - \frac{S_i s_j^2 + S_j s_i^2}{s_i + s_j} \Bigg) \Bigg]^{-\frac{d}{2}} \Bigg\}. \end{aligned} \tag{A.12}$$

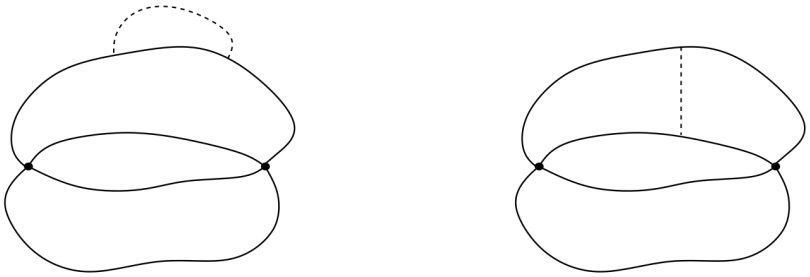

(a) (b)

Figure A.4: First order diagram types for the watermelon network. **(a)** Diagram of type A, obtained by joining two points on the same branch. **(b)** Diagram of type B, obtained by connecting two different chains. Note that the figure is on a plane, but our networks are working in 3 dimensions, so the "order" in which the branches are displayed is not relevant: each interaction line adds only one independent loop.

In [2] one can also find the ϵ expansion of these integrals and the calculation of the fixed value of the amplitude $\mathscr{A}$ that appears in the asymptotic factorization over the vertices (see chapter 2). Again, one could check that when $S_i = S$, $i = 1, \ldots, 4$, the expected scaling contribution of the loops is recovered.

Appendix B

Calculation of the Mean Value of the Total Length of Links (Described by Networks) in the Asymptotic Limit

In chapter 2 we have seen how, in the asymptotic limit $N \gg 1$, we can describe the number of configurations of the networks with vertex topology $\mathscr{G}$ and total length N with the power law

$$\mathscr{Z}_N(\mathscr{G}) \sim \mu^N N^{\gamma_{\mathscr{G}}-1} \qquad (N \gg 1), \tag{2.3}$$

where $\gamma_{\mathscr{G}}$ is a suitable critical exponent.
In chapter 4, we showed that the BFACF algorithm we used for a system made of two linked loops with lengths N_1 and N_2, converges to a stationary limit distribution on the configuration space Ω that reads, for a fixed topology τ,

$$\pi_\tau(\omega) = \frac{1}{G_q(K,\tau)}(N_1+N_2)^q K^{(N_1+N_2)}\chi(\tau(\omega),\tau), \tag{4.6}$$

where K and q are parameters of the simulation, $\omega \in \Omega$, and

$$G_q(K,\tau) = \sum_{N_1,N_2} \mathscr{Z}_{N_1,N_2}(\tau)(N_1+N_2)^q K^{(N_1+N_2)}.$$

As we explained in chapter 3 we associated a couple of unknotted linked polygons with the scaling law of networks. Hence, we are going to combine this distribution with the topology dependent approximation[1]

$$\mathscr{Z}_N(\tau) \approx A(\tau)\mu(\tau)^N N^{\gamma(\tau)-1} \qquad (N \gg 1) \tag{B.1}$$

[1] In chapter 3 we stated that we are treating a fixed topology by adding in the coefficients and exponent of the scaling law a dependence on it.

in order to calculate $\langle N\rangle_q(K,\tau)$. Let us start from the normalization factor[2]

$$G_q(K,\tau) \approx A(\tau)\sum_{N=N_{min}(\tau)}^{\infty} N^{\gamma(\tau)+q-1}(\mu(\tau)K)^N. \tag{B.2}$$

Since we are in the $N \gg 1$ limit, we can approximate the sum in this definition with an integral:

$$G_q(K,\tau) \approx A(\tau)\int_0^{\infty} dN N^{\gamma(\tau)+q-1}(\mu(\tau)K)^N. \tag{B.3}$$

Remembering the definition of the Gamma function,

$$\int_0^{\infty} dt e^{-st}t^{\alpha} = \frac{\Gamma(\alpha+1)}{s^{\alpha+1}},$$

which is a convergent integral for $\alpha > 0$, we get, for $\gamma(\tau)+q-1>0$,

$$G_q(K,\tau) \approx A(\tau)\frac{\Gamma(\gamma(\tau)+q)}{[\ln(\mu(\tau)K)^{-1}]^{\gamma(\tau)+q}}. \tag{B.4}$$

Given that we choose K so that $(\mu(\tau)K)^{-1} \approx 1$ (see chapter 6), we can approximate $\ln(\mu(\tau)K)^{-1} \approx (1-\mu(\tau)K)$, so we have

$$\begin{aligned} G_q(K,\tau) &\approx \tilde{a}(\tau)(1-\mu(\tau)K)^{-\gamma(\tau)-q} \\ \tilde{a} &= A(\tau)\Gamma(\gamma(\tau)+q). \end{aligned} \tag{B.5}$$

Using this approximation, we can extract the mean value of N from the relation

$$\langle N\rangle_q(K,\tau) = \frac{\sum_{N=N_{min}(\tau)}^{\infty} N\mathscr{Z}_N(\tau)N^qK^N}{G_q(K,\tau)} = \frac{K}{G_q(K,\tau)}\frac{\partial G_q(K,\tau)}{\partial K}. \tag{B.6}$$

$$\frac{\partial G_q(K,\tau)}{\partial K} \approx \tilde{a}(\tau)(\gamma(\tau)+q)\mu(\tau)(1-\mu(\tau)K)^{-\gamma(\tau)-q-1}, \tag{B.7}$$

so we get

$$\begin{aligned} \langle N\rangle_q(K,\tau) &\simeq a(\tau)\mu(\tau)K(1-\mu(\tau)K)^{-1} \\ a(\tau) &= \gamma(\tau)+q. \end{aligned} \tag{B.8}$$

[2]Forgetting about the characteristic function χ.

Bibliography

[1] Orlandini E., Tesi M. C., Janse van Rensburg E. J. and Whittington S. G. *Asymptotics of knotted lattice polygons*, *J. Phys. A: Math. Gen.* **31**, 5953 (1998)

[2] Douplantier B., *Statistical Mechanics of Polymer Networks of Any Topology*, *J. Stat. Phys.* **54**, 581, (1989)

[3] de Gennes P. G., *Scaling Concepts in Polymer Physics*, *Phys. Lett.* **A38**, 339 (1972)

[4] Brèzin E., Le Guillou J. C. and Zinn-Justin J., in *Phase Transitions and Critical Phenomena* Vol. 6, Domb C. and Green M. S. eds. (Academic Press, New York, 1976)

[5] Guttmann A. J., *J. Phys. A: Math. Gen.* **22**, 2807 (1989)

[6] Li B., Madras N. and Sokal A. D., *J. Stat. Phys.* **80**, 661 (1995)

[7] Guida R., Zinn Justin J., *Preprint SPHT T97/040* (1997)

[8] Soteros C. E., Sumners D. W. and Whittington S. G., *Math. Proc. Camb. Phil. Soc.* **111**, 75 (1992)

[9] Hammersley J. M., *The number of polygons on a lattice*, *Proc. Camb. Phil. Soc.* **57**, 516 (1961)

[10] Douplantier B., *Phys. Rev. Lett.* **57**, 941 (1986)

[11] Edwards S. F., *Proc. Phys. Soc. Lond.* **85**, 613 (1965)

[12] des Cloizeaux J., *J. Phys.* (Paris) **42**, 635 (1981)

[13] Bergère M. and David F., *J. Math. Phys.* **20**, 1244 (1979)

[14] Kunh W., *Kolloid Z.* **68**, 2 (1934)

[15] Li B., Madras N. and Sokal A.D., *J. Stat. Phys.* **80** 661 (1995)

[16] Häggström O., *Finite Markov Chains and Algorithmic Applications*, Cambridge University Press, 609 (2002)

[17] Berg B. and Foester D., *Random paths and random surfaces on a digital computer*, *Phys. Lett.* **B106**, 323 (1981)

[18] Aragao de Carvalho C. and Caracciolo S., *A new Monte Carlo approach to the critical properties of self-avoiding random walks*, *J. Phys.* (Paris) **44**, 323 (1983)

[19] Janse van Rensburg A.W.and Whittington S.G., *The BFACF algorithm and knotted polygons*, *J. Phys. A: Math. Gen.* **24**, 5553 (1991)

[20] Metropolis N., Rosenbluth A.W., Rosenbluth M.N., Teller A.H. and Teller E., *J. Chem. Phys.* **21**, 1087 (1953)

[21] Sokal A.D., *Monte Carlo Methods in Statistical Physics: Foundations and New Algorithms lectures at the Cargèse Summer School on "Functional Integration: Basics and Applications"* (1996)

[22] Madras N. (1986) and Madras N. and Slade G., *The Self-avoiding Walk* (Boston: Birkhauser, 1993)

[23] Reidemeister K., *Knotten und Gruppen*, *Abh. Math. Sem. Univ. Hamburg* **5**, 7 (1927)

I thank Prof. Orlandini for assisting me in this work.

Andrea